Development of a Reagentless Electrochemical Glucose Sensor

Nassima Naas

A Thesis

in

The Department

of

Chemistry and Biochemistry

Presented in Partial Fulfillment of the Requirements
for the degree of Master of Science at
Concordia University
Montreal, Quebec, Canada

March 2006

Your file Votre référence
ISBN: 0-494-14230-8
Our file Notre référence
ISBN: 0-494-14230-8

Abstract

Development of a reagentless electrochemical glucose sensor

Nassima Naas

Glucokinase catalyzes the phosphorylation of glucose using ATP and magnesium cations. Dr. M.Trifiro's research group (at the Lady Davis institute at the Sir Mortimer B.Davis Jewish General Hospital) have re-engineered this enzyme and obtained a pure glucose binder that does not need any ATP or Mg^{2+} to be present.

In this work, developing a reagentless electrochemical glucose sensor by immobilizing the wild type enzyme onto semi-conductor silicon chips as well as screen-printed carbon electrodes, was attempted.

In the first immobilization procedure, the substrates were modified with nitrobenzenediazonium and glutaraldehyde. The electrodes were then put in contact with a glucose solution. The changes introduced to the surface were monitored using impedance measurements, which show that the enzyme was successfully immobilized, but its active site seems to be unavailable for glucose binding.

In the second immobilization procedure, the substrates were modified with an amine terminated NTA ligand. This was done by trying to generate and reduce an in-situ diazonium moiety, after reaction with $NaNO_2$. This approach failed because there was no aniline moiety in the ligand, which according to literature, is crucial.

In the last immobilization procedure, the substrates were oxidized in the presence of 1-Ethyl-3-(3-dimethylaminopropyl)-carbodiimide and then the NTA ligand was added. Electrodes were then loaded with nickel cations. The glucokinase was tagged with a 6-histidine tail, which was expected to coordinate to Ni^{2+}, thus ensuring the availability of the active site. Results indicated that the electrodes were successfully modified and showed to be sensitive to the presence of glucose.

Acknowledgements

I would like to thank Dr.Lawrence for giving me the opportunity to work on such a fascinating project. His help and inspiring attitude will never be forgotten. I would also like to thank Dr. Mark Trifiro and his group, especially Ms. Rose Sidloi. Your help, support and guidance are greatly appreciated.

I would like to thank Dr. C. DeWolf and Dr. S. Robidoux for serving on my research committee.

I would like to thank my friends and colleagues at Concordia University for making my time there so special: Marika Dochia, Petrina Kamya, Nancy Austin and Yvonne Jost.

Finally, I would like to dedicate this thesis to my very supportive family: my mother and father: Zakya and Abderrahmane, my sisters: Lamia and Keltoum, and my brother: Mehdi.

Table of Contents

List of Figures

List of Tables

List of Symbols

ATP:	Adenosine triphosphate
C:	Capacitance
CB:	Conduction band
C_d:	Capacitance of the double layer
CE:	Counter electrode.
ct:	Charge transfer
CV:	Cyclic voltammetry
DCCT:	Diabetes Control and Complications Trial
DNA:	Deoxyribonucleic acid
E:	Energy
EDC:	1-Ethyl-3-(3-dimethylaminopropyl)-carbodiimide
E_f:	Fermi level
EIS:	Electrolyte / Insulator / Semi-conductor
E_{reox}:	Redox potential
ϵ:	Dielectric constant
ϵ_0:	The permittivity of free space
F:	Faraday's constant
f:	Linear frequency
GK:	Glucokinase
GOD:	Glucose Oxidase
I:	Current
IDDM:	Insulin Dependent Diabetes Mellitus

NIDDM:	Non-insulin Dependent Diabetes Mellitus
NTA:	Nitrilotriacetic acid
R:	Resistance or gas constant
R_{Ω} :	Resistance of the electrolyte
R_{ct}:	Charge transfer resistance
Ref:	Reference
SCE:	Saturated Calomel Electrode
SPE:	Screen printed carbon electrode
T:	Temperature
VB:	Valence band
V_{fb}:	Flat band potential
V:	Potential
WE:	Working electrode
ν:	linear potential scan rate
ω:	Angular frequency
Z:	Impedance
Z_w:	Warburg Impedance

Chapter 1:

Introduction

1.1. Diabetes Overview

1.1.1. What is diabetes?

Glucose is a carbohydrate and is the main source of energy of most living organisms, including humans. Insulin is a hormone produced by the beta cells in the pancreas and is the glucose regulator of the body. Its function is to pass glucose from the blood stream into the body cells. Diabetes mellitus is a group of diseases caused by high levels of blood glucose resulting from a total, or partial, lack of insulin (1, 2). There are two main types of diabetes:

- **Type1 diabetes**, also known as insulin dependent diabetes mellitus (IDDM) or juvenile onset diabetes, accounts for about 5 to 10% of diagnosed cases. It is considered as an autoimmune disease where the immune system attacks the pancreatic beta cells and destroys them. The production of insulin is then stopped, resulting in high blood glucose levels, which, if untreated, can cause the patient to fall into a fatal coma. This type is mostly treated with insulin therapy. Patients must inject themselves several times a day to survive.

- **Type2 diabetes**, also known as non insulin-dependent diabetes (NIDDM), is the most common form of the disease and accounts for 90 to 95% of diagnosed cases. In this type, insulin is usually produced but is not effectively used by the body. Thus the main source of fuel, glucose, cannot be efficiently used. Treatment usually consists of a strict diet and exercise program and sometimes insulin therapy.

Both types of diabetes can induce very serious complications, even if treatment is administered. These include: heart disease, stroke, high blood pressure, blindness, kidney disease, nervous system disease, amputations, dental disease and complications of pregnancy.

1.1.2. Statistics.

The number of people with diabetes is continuously growing. According to the World Health Organization, 150 million people have diabetes worldwide (2). This number is expected to double by the year 2025. By then, most people with diabetes in developed countries will be over the age of 65 whereas in developing countries most will be between the age of 45 and 64.

In 1994, 3.0% of Canadians of all age groups were diagnosed with the disease. In 2001, they were 4.1%, which represents 1,063,698 persons. Older people are more susceptible to the disease. In 2001, 12.5% of Canadian men and women over the age of 75 were diagnosed as being diabetic (3).

In the United States, in 1998, 15.7 million people – 5.9% of the population – had diabetes. The disease is especially devastating in communities like American Indians where the number of cases ranges from 5% up to 50% of the population. In North America alone, 5 million people are insulin dependent (1).

These numbers are overwhelming and reflect all the effort that has been done in the scientific community to develop a better treatment, a better understanding of the causes of the disease and to eventually find a cure.

1.2. Methods of glucose monitoring

1.2.1. Laboratory methods

Analytical laboratory techniques for glucose testing are very accurate (with errors less than 1%) and are considered as standards for comparison with new methods and devices under development (4- 6).

A famous long-term ten-year study (completed in 1993), called the Diabetes Control and Complications Trial (DCCT), focused on the comparison between two groups of IDDM diabetics. One group underwent a treatment called "intensive management" and the other a treatment called "standard management". The former group was the one who achieved the tightest control of glucose levels and consequently had significantly lower rates of diabetes-related complications. Continuous monitoring was concluded to be the best way to control the disease. Researchers then focused on developing biosensors since they present the highest potential for continuous monitoring (1, 6, 7).

1.2.2. Biosensors

1.2.2.1. What is a biosensor?

A biosensor is a device used to detect and, usually, quantify a specific analyte. It is composed of two parts. The first one is a biological component (e.g.: enzyme, antigen...etc) that recognizes selectively the desired analyte (e.g.: glucose, urea, toxic metal ions...etc). The second component is a transducer that converts the recognition event into a readable signal (8-11).

1.2.2.2. Biosensors for glucose monitoring

The first glucose biosensors were bedside devices, developed in the late seventies, which enabled blood glucose concentrations to be measured transiently under clinical conditions. Nowadays, these biosensors have been miniaturized to the point of becoming wearable as a wristwatch. They are easily used by patients for home monitoring (6).

Despite all this progress, there are still several disadvantages related to these sensors. First, when patients need to verify their glucose level, they have to draw a blood sample, usually from the index finger. This can become very painful because it is done several times a day. Puncturing the tissue is also related to scarring and infection. Developing a biosensor that would eliminate this step is the goal of many research groups in this field.

Another disadvantage of present day biosensors is that, even though their response time is short (less than a minute), they are still not considered continuous, real-time monitoring devices. They only allow retrospective analysis. Last but not least, self-monitoring by patients is for now impossible during their sleep (12).

Researchers are well aware of these problems and realize that the ultimate solution would be to create an implantable biosensor. This idea was reinforced when implantable insulin pumps were developed to relieve the patients from having to inject themselves with insulin several times a day. These pumps are now stable within the body for up to ten years. However, they still have to be controlled externally by the patient or the physician.

In the late seventies, the concept of the "Artificial Beta Cell" was introduced. The goal was to create "a technical closed loop composed of the sensor as a transmitter and the pump as a driver, both being connected by a special computer controlling the mathematical glucose/insulin relation." (6, 13) This is the Holy Grail for scientists in diabetes research. Developing such a device would be the closest thing to a cure for the disease.

Implantable biosensors are being developed but have not yet crossed the experimental stage. Most of them are amperometric and use enzymatic reactions for the detection of glucose. Glucose oxidase (GOD) is the enzyme that is of choice for this purpose. This is because it catalyzes the oxidation of glucose through a reaction that generates H_2O_2, which can be easily oxidized at a +700 mV polarized electrode vs SCE as reference (5, 6):

$$\text{D-glucose} + O_2 \xrightarrow{\text{GOD}} \text{Gluconic acid} + H_2O_2 \qquad \text{(reaction 1)}$$

$$H_2O_2 \xrightarrow{+700\ \text{mV}} 2\,e^- + 2\,H^+ + O_2 \qquad \text{(reaction 2)}$$

Enzymatic reactions can be very complicated and, as shown with the reactions above, need reagents in order for the catalysis to occur. The resulting biosensor will need replenishment with these extra reagents. This can be tedious and painful for the patient if the biosensor is already implanted.

Optical implantable biosensors based on fluorescence are under development. The probe is subcutaneously implanted in order to measure interstitial glucose. The data is transferred wirelessly to an external reader worn as a wristwatch. Animal testing with these devices is very promising. However, their major drawback is their significantly high cost (14).

1.3. Glucokinase

1.3.1. What is glucokinase?

Hexokinases are enzymes that catalyze the phosphorylation of glucose into glucose-6-phosphate in the presence of ATP and magnesium cation (15, 16):

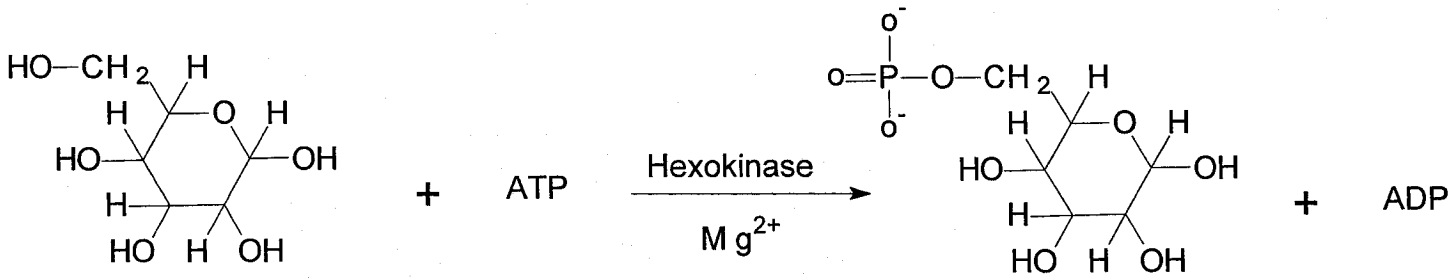

Figure 2.3.1.1: phosphorylation of glucose by hexokinase.

Human hexokinase IV, usually referred to as glucokinase, is a 50 kD enzyme found in the liver and in the ß islets of the pancreas where it is believed to be the glucose sensor. It catalyzes the ATP-dependent phosphorylation of glucose into glucose-6-phosphate as the first step and also the first rate-limiting step in the glycolytic pathway. It has low-affinity to glucose (K_m = 5 to 8mM) compared to other hexokinases (K_m = 20 to 130 µM). It also has a high specificity for glucose, as it is inactive with other sugars like mannose and fructose, unlike other hexokinases (17-20). Three-dimensional molecular modeling studies show that it has two binding sites: one for ATP and Mg^{2+}, and a second one for glucose. Kinetic and crystallographic studies suggest that ATP binding occurs independently of glucose binding. This implies that if the binding site of ATP were to be removed, glucokinase would keep its glucose binding ability (12, 20)).

1.3.2. Re-engineering of glucokinase

Using DNA recombinant technology, Dr. Mark Trifiro's research group at the Lady Davis Institute (Montreal Jewish General Hospital) was able to re-engineer glucokinase and create mutant enzymes that lack the ATP binding site. Enzymatic activity is then suppressed and, for the first time, a pure glucose receptor is obtained (enzymes are not considered pure receptors because they only bind to glucose in order to catalyze a reaction and obtain a new molecule). This receptor can be incorporated in a biosensor to detect and measure blood glucose levels (12).

1.4. Goals and outline of the project.

In this project, we will attempt to develop a novel reagentless glucose biosensor. It is described as "reagentless" because its biological component, the mutated glucokinase described above, requires no other chemicals in order to bind to glucose. Eventually, the sensor interconnected to an insulin pump could be implanted into patients. No replenishments would be needed and a real time continuous glucose monitoring system can be envisaged.

Our experience with biosensors using impedance is extensive. Our research group has focused for years on the development of DNA sensors. This was done by immobilizing single DNA strands onto modified semiconductor electrodes. The sensor is then put in contact with a solution of single stranded DNA that can hybridize with the immobilized ones. Matches and mismatches can thus be detected (8-10, 21).

Similarly, in this project, the wild type glucokinase will be immobilized onto modified silicon semiconductor electrodes and onto carbon paste screen-printed electrodes. The enzyme electrodes will then be put into contact with a glucose solution. The changes that will occur at the surface of these electrodes will all be monitored using impedance (Mott-Shottky and Nyquist). Evaluation of the activity of the immobilized enzyme using standard enzyme assay methods, will also be attempted.

The reason that the wild type enzyme is used instead of the mutant, is that the latter is quite costly. It would be more convenient to optimize the sensor with the wild type since it is expected to behave in a similar fashion as the mutated enzyme.

Chapter 2:

Theory

2.1. EIS structure

The electrolyte insulator semiconductor (EIS) structure represents the interface between a semiconductor and a solution containing a redox couple (an electrolyte). The Fermi level, E_f (energy at which the probability of occupation by electrons is ½), and the redox potential (E_{redox}) are equivalent to the chemical potentials of the semiconductor and of the solution, respectively (22, 23).

If a semiconductor with a high E_f is put in contact with a solution of a lower E_{redox}, electrons will flow spontaneously from the semiconductor to the solution in order to equilibrate the chemical potentials (figure 2.1.1). This will go on until E_f and E_{redox} become equal (24).

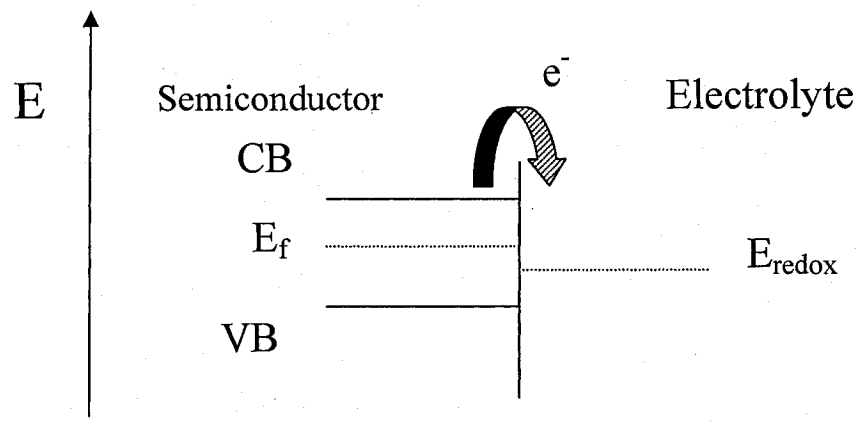

Figure 2.1.1: Electronic flow through the semiconductor / electrolyte interface (CB is the conduction band and VB is the valence band of the semiconductor).

As the electrons flow, an excess of positive charges appears in the semiconductor near the interface. Consequently, an excess of negative charges appears in the solution, also near the interface. This is symbolized by bending the bands of the semiconductor (figure 2.1.2). The electrolyte contains a lot more charge carriers than the semiconductor and so the described electron flow will have little effect on their number. This is why there is no band bending in the electrolyte (25). There comes a point where so many electrons have gone through, that the excess of negative charges in the solution now blocks their flow. The system has reached equilibrium. An electric field is thus created between the semiconductor and the electrolyte. The region where the bands are bent contains no charges and is called the "depletion region" or "space charge layer". If an electron was to be forced in it, it will follow the direction of the electric field and go towards the bulk of the semiconductor. A positive charge would go towards the solution. The space charge region has a real physical thickness and behaves like a dielectric (an insulator) (24, 25).

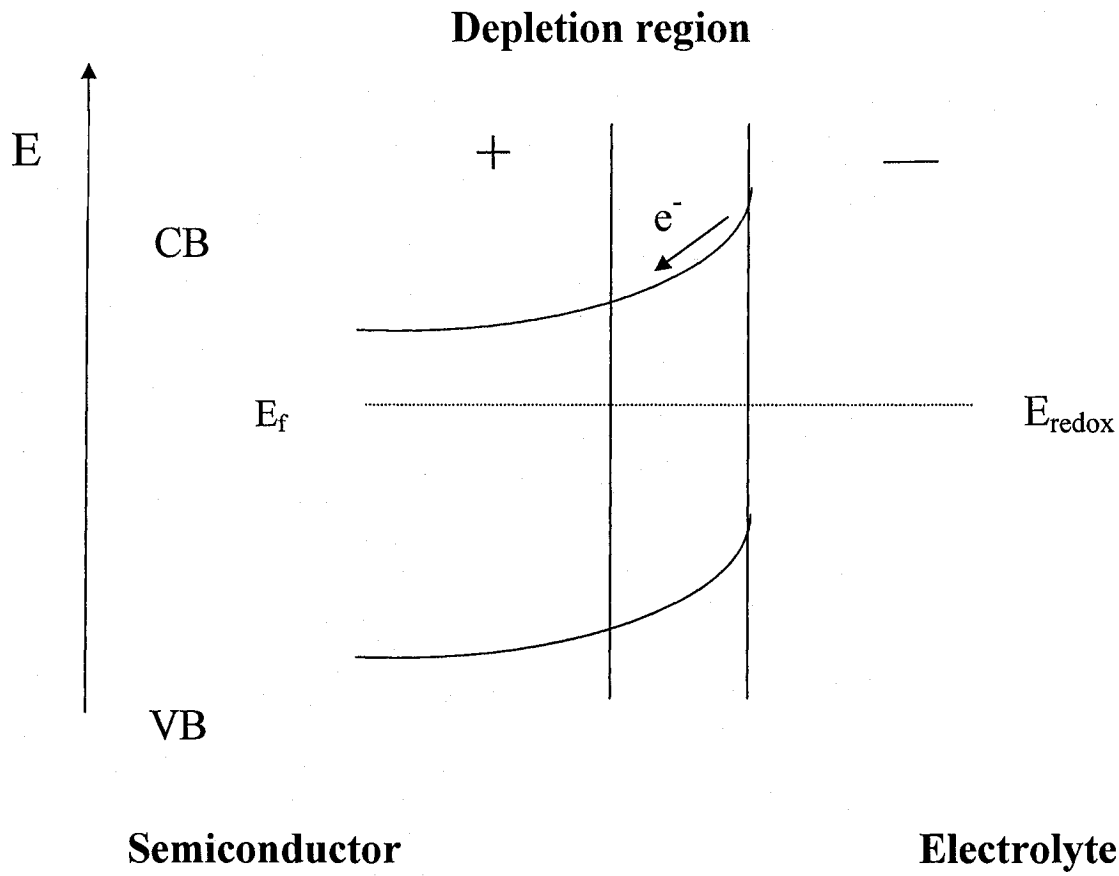

Figure 2.1.2: Semiconductor / electrolyte interface, at equilibrium. VB is the conduction band and CB is the conduction band.

2.2. Impedance Measurements

Resistance is defined as the ability of a material to resist the flow of electrical current. Ohm's law relates the current (I), potential (V) and resistance (R) according to the following equation:

$$V = R \times I \qquad \text{(equation 1)}$$

However, it is important to note that this relationship is only applicable to one type of circuit element, the ideal resistor, which has the following properties (26):

- It obeys Ohms' law at all current and voltage levels.
- Its resistance value is independent of frequency when an alternating current (AC) is applied.
- AC current and voltage signals, through a resistor, are in phase with each other.

In reality, however, these conditions are rarely fulfilled. The resistance in Ohm's law is thus replaced with another property, impedance. Ohm's law takes on the form:

$$\tilde{V} = Z \times \tilde{I} \qquad \text{(equation 2)}$$

In equation 2, the impedance, Z, the alternating voltage, $\tilde{V}$, and alternating current, $\tilde{I}$, are all complex numbers composed of a real part (subscript "r") and an imaginary one (subscript "i"):

$$(V_r + iV_i) = (Z_r + iZ_i) \times (I_r + iI_i) \qquad \text{(equation 3)}$$

By re-arranging equation 3, the real and imaginary parts of the impedance can be expressed as (21):

$$Z_r = \frac{V_r I_r + V_i I_i}{I_r^2 + I_i^2} \qquad Z_i = \frac{V_i I_r - V_r I_i}{I_r^2 + I_i^2} \qquad \text{(equation 4)}$$

The imaginary part of the impedance, Z_i, is especially interesting because it yields information about the capacitance within the system under study, C, through the following equation (23):

$$Z_i = 1/(\omega \times C) \qquad \text{(equation 5)}$$

Where ω is the angular frequency of the alternating voltage. It is related to the linear frequency, f, through the following equation:

$$\omega = 2 \times \pi \times f \qquad \text{(equation 6)}$$

The capacitance of the system is related to the applied potential through the Mott-Schottky equation:

$$1/C^2 = \{2(V-V_{fb})\} / (\epsilon_0 \epsilon N_D) \qquad \text{(equation 7)}$$

In equation 7, V is the applied potential and V_{fb} is the flat band potential. The latter is defined as the externally applied potential at which the band bending, illustrated in figure 2.1.2, is eliminated. ϵ_0 is the permittivity of free space and ϵ is the dielectric constant of the semiconductor. N_D is the density of the dopant atoms (example: phosphorus donor atoms for n-type semiconductivity). Equation 7 implies that a plot of $1/C^2$ versus the applied potential would be a straight line (23, 24).

2.3. Impedance Measurements at a Semiconductor Electrode

If the system in figure 2.1.2 is put in an electric circuit with a source (potentiostat) and a reference electrode, electrochemical measurements can be realized (figure 2.3.1). When a negative potential is applied, electrons are pushed into the semiconductor. If this potential were negative enough, there would be so many electrons that were pushed into the semiconductor that they would go through the interface and end up in the solution. This can cause unwanted faradaic phenomena (example: reduce or oxidize electro-active species present in the solution). To avoid this, a dielectric layer is deposited on the semiconductor to hinder any transfer of electrons into the solution. The response measured by the potentiostat, would be the accumulation of charges at the interface, at either side of the dielectric layer. In other words, the potentiostat would be measuring a capacitance.

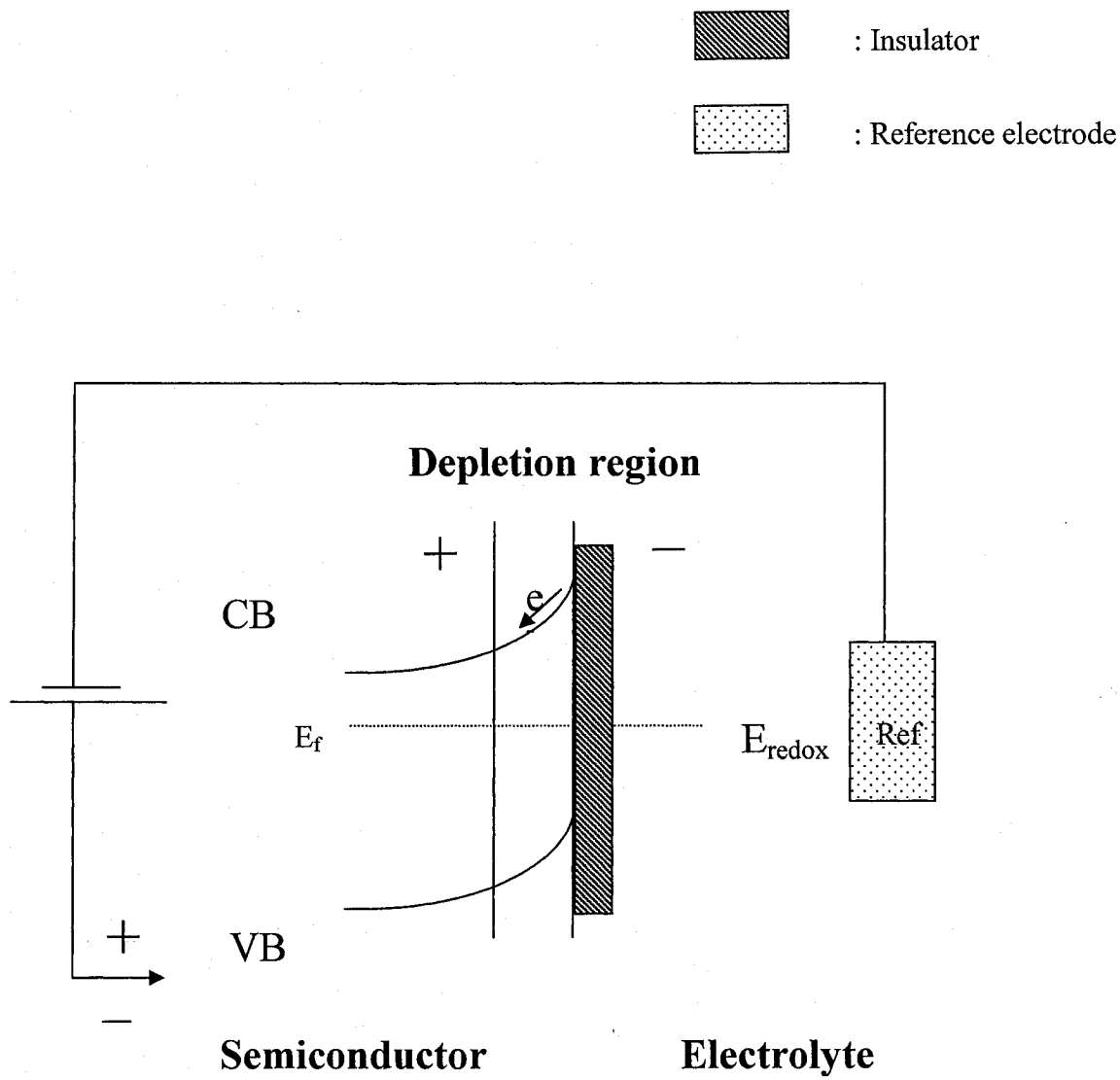

Figure 2.3.1: Semiconductor / electrolyte interface in a circuit with a source and a reference electrode

It is important to determine whether or not the capacitance measured by the potentiostat gives direct information on transformations at the surface of the semiconductor. To provide an answer, an analysis of all the capacitances that exist within the semiconductor is needed. To achieve this, it is common for electrochemists to use equivalent circuits. Figure 2.3.2 illustrates the equivalent circuit of our system (23, 25).

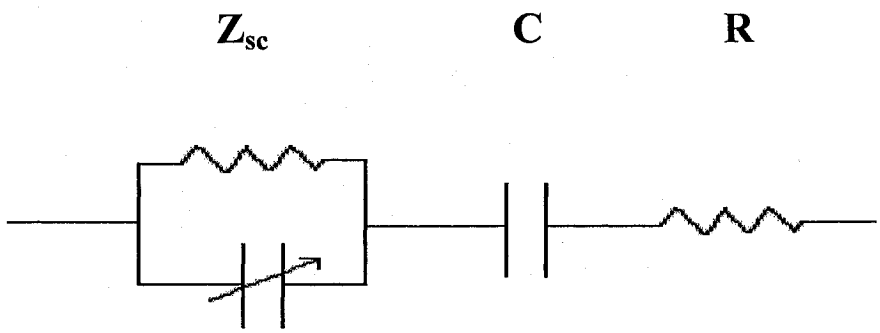

Figure 2.3.2: Equivalent circuit of the system in figure 2.1.3.

In figure 2.3.2, R is the resistance of the solution, C is the capacitance of the insulating layer and Z_{SC} is the impedance of the semiconductor. The latter is composed of a resistance and a variable capacitance. From this circuit, the overall capacitance can be expressed as:

$1/C = 1/C_{SC} + 1/C_{insulator}$ (equation 8)

The insulating layer being considerably thicker than the space charge layer, the capacitance of the latter is much smaller:

$C_{SC} << C_{insulator}$, so $1/C_{SC} >> 1/C_{insulator}$, and $1/C \approx 1/C_{SC}$.

Recall, from equation 5, that Z_i is directly related to 1/C. This implies that the imaginary component of the impedance measured by the potentiostat will be directly related to the capacitance of the space charge layer of the semiconductor. In conclusion, we will be able to extract direct information about the surface of the semiconductor by measuring the imaginary component of the impedance. This is done by applying a low frequency alternating voltage, superimposed onto a potential ramp. The real and imaginary components of the impedance are calculated by the computer program (Voltamaster) using equation 4.

Figure 2.3.3 is an example of the type of data collected after one run of impedance measurements at a semiconductor electrode.

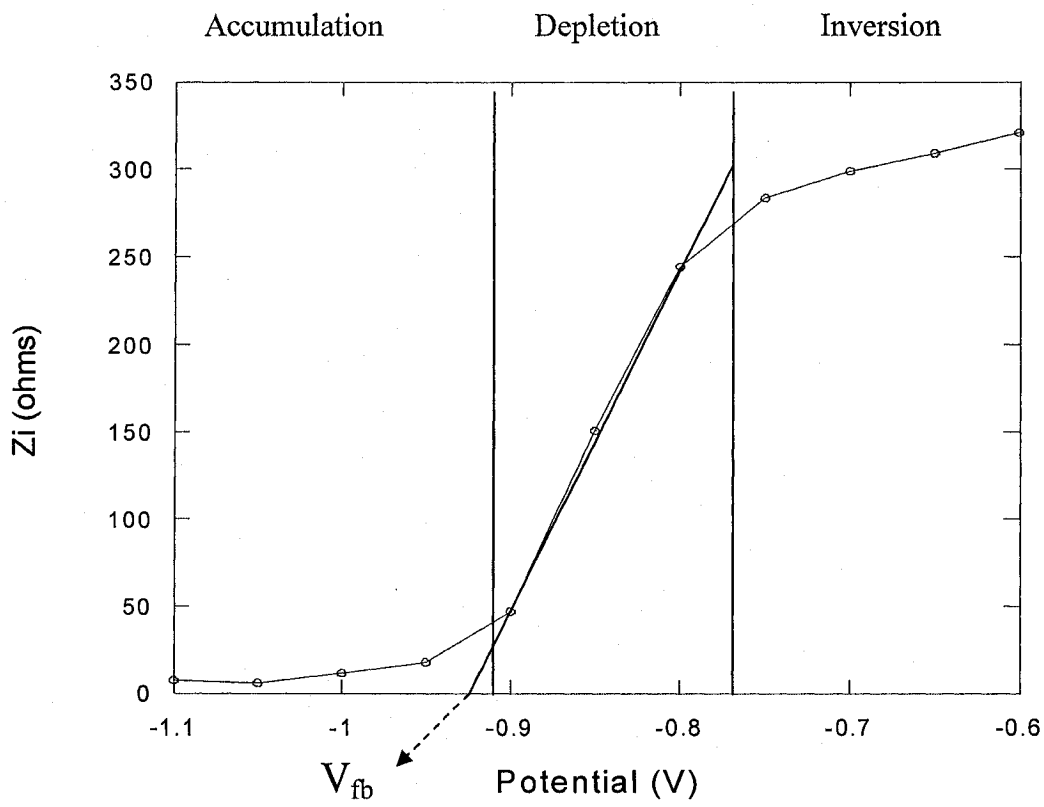

Figure 2.3.3: Mott-Schottky plot at an n-type semiconductor electrode.

This S shaped plot is divided into three distinct regions called regimes. At very negative potentials, electrons are being pushed into the semiconductor and so they accumulate at the interface between the semiconductor and the insulator. In the electronic structure, the bands are bent upwards (figure 2.3.4). This part of the plot is called the accumulation regime (8-10, 24, 25).

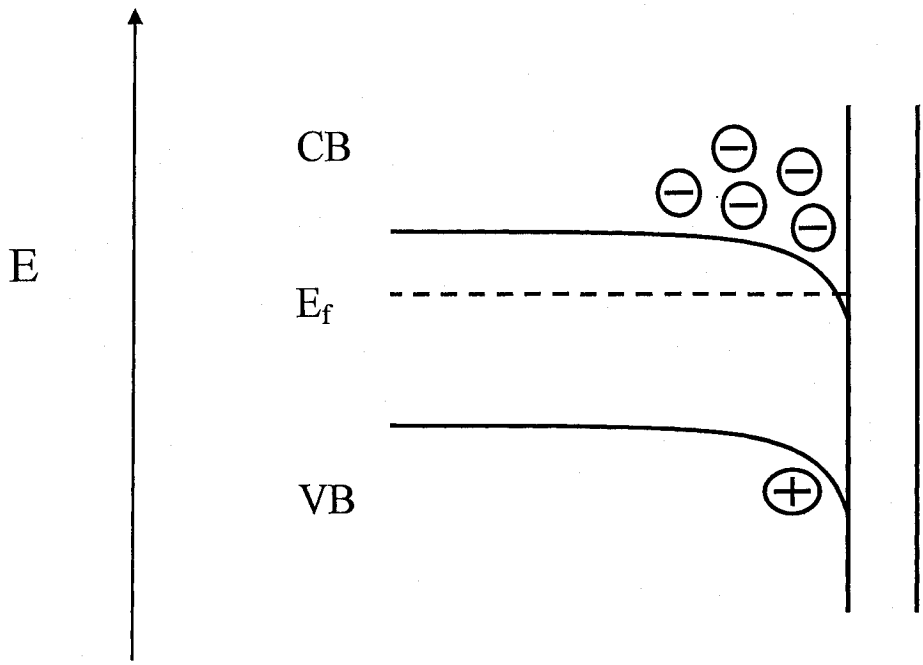

Figure 2.3.4 : Accumulation regime in an n-type semiconductor.

As the ramping DC potential becomes more and more positive, electrons are being gradually withdrawn from the semiconductor. The bands start bending downwards and this is called the depletion regime (figure 2.3.5).

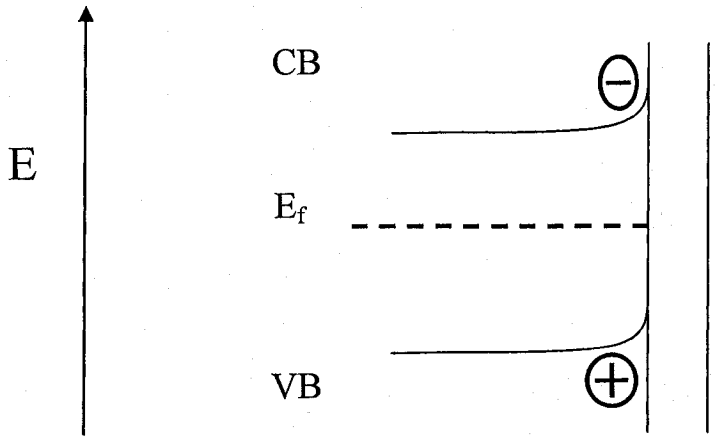

Figure 2.3.5 : Depletion regime in an n-type semiconductor.

At even more positive potentials, so many electrons have been withdrawn from the semiconductor, that the positive charges are the ones accumulating at the surface. The bands are now more curved. This is called the inversion regime (figure 2.3.6).

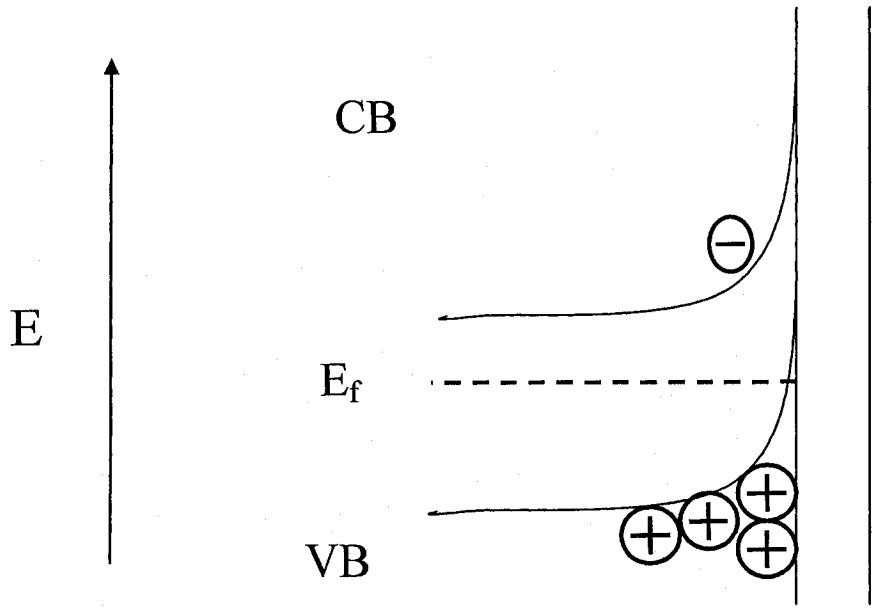

Figure 2.3.6 : Inversion regime in an n-type semiconductor.

2.4. Impedance Measurements at a Conductor Electrode.

As stated in the introduction section, two types of electrodes will be used in this project: semiconductor Si and Carbon paste screen-printed electrodes (SPEs). The latter are conducting, which means that their electronic structure differs from the one described above (figure 2.1.1), because their CB and VB overlap (figure 2.4.1).

When this type of electrode is placed in contact with an electrolyte, electrons will flow until E_f and E_{redox} become equal. Depending on the charge of the surface of the electrode, ions from the solution will adsorb onto it. The latter will attract counter ions and so on until electro-neutrality is reached. A double layer is thus formed (22, 23, 26).

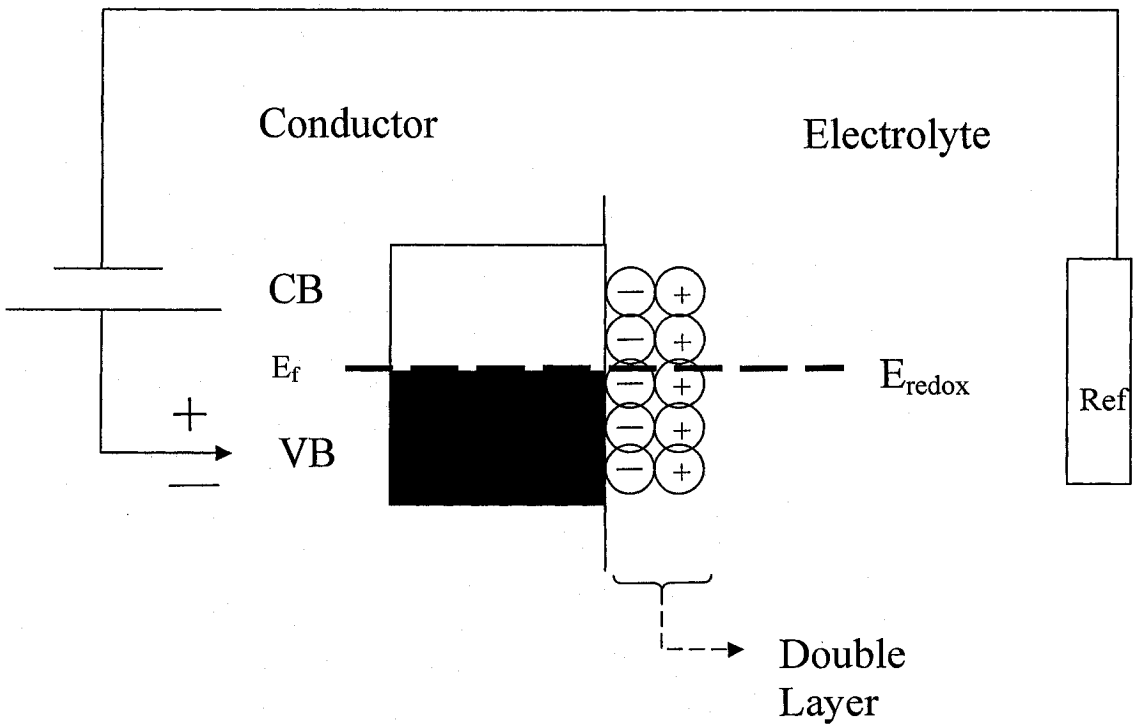

Figure 2.4.1: Conductor electrode in contact with an electrolyte and put in a circuit.

As shown in figure 2.4.1, the system can be incorporated in an electrical circuit, with a source and a reference electrode. Figure 2.4.2 shows the new equivalent circuit for this new system (25).

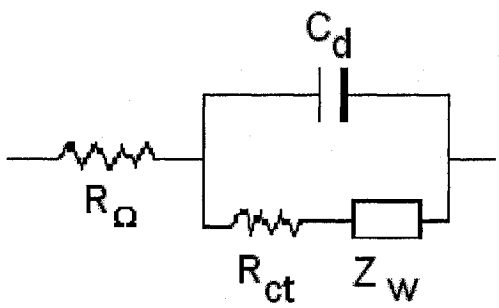

R_Ω: resistance of electrolyte

C_d: capacitance of the double layer

R_{ct}: charge transfer resistance

Z_w: Warburg Impedance

Figure 2.4.2: equivalent circuit of an SPE electrode in contact with an electrolyte.

Z_W is called the Warburg impedance and reflects the resistance due to the mass transfer or diffusion (23, 26).

Since we are now dealing with a conductor electrode, there is no depletion region, and so capacitance measurements (Mott-Schottky) cannot be realized. Instead, the resistance to the flow of electrons can be measured. To do this, the DC potential is kept constant and the frequency of the AC potential is varied. Z_i is plotted versus Z_r going from high AC frequencies to lower ones. This type of graph is called a Nyquist plot and Figure 2.4.3 shows a typical one (29).

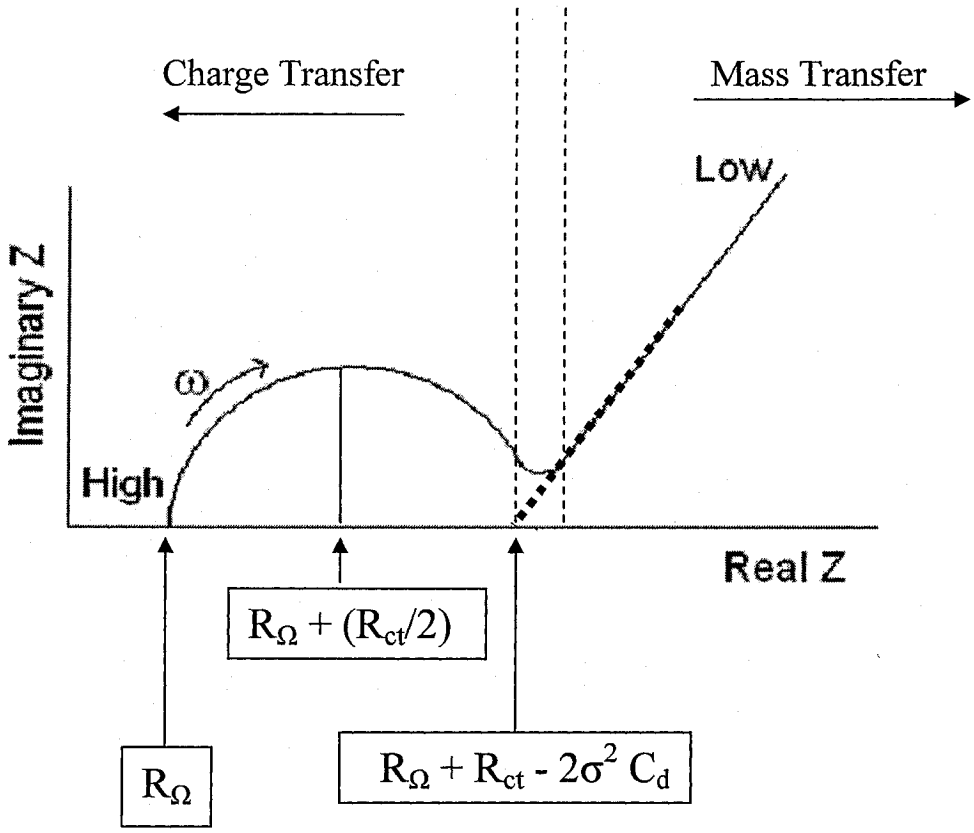

Figure 2.4.3: Typical Nyquist plot (28).

The plot in figure 2.4.3 can be divided into two regions. At high ω, a semi-circle is obtained centred at the point: $((R_\Omega + (R_{ct}/2));0)$ and with a radius value of $R_{ct}/2$. In this region, the polarization of the interface is very brief and so electrolyte ions don't have to diffuse very far. Most of the impedance is due to the charge transfer resistance.

On the other hand, at low frequencies, reactants are forced to diffuse over longer "distances in the electrolyte" to get to the surface of the electrode, and so most of the impedance is due to this diffusion. The latter is called resistance to mass transfer or the

Warburg impedance. As shown in figure 2.4.3, the extrapolation of this linear part to the Z_r axis is a point where:

$$Z_r = R_\Omega + R_{ct} - 2\sigma^2 C_d$$

With: $\sigma = nF\nu / RT$ (equation 9)

n = number of electrons involved

F = Faraday's constant

ν = linear potential scan rate

R = Gas constant

T = Temperature

This extraploation generates direct information on the double layer adsorbed onto the surface of the electrode (C_d).

2.5. Cyclic Voltammetry.

Cyclic voltammetry, CV, is an important electrochemical method used to characterize the redox behavior of an electroactive species. It can yield information on the rate of a reaction, its mechanism and its reversibility. In this technique, a linear DC potential ramp is applied to an electrochemical cell and the resulting current is measured. First, the potential is usually scanned starting with a voltage at which no reaction occurs, E_1, and ending at a more negative potential E_2. Second, the potential scan is reversed from E_2 to E_1 (figure 2.5.1) (22, 23). This procedure can be repeated several times. The scan rate υ (usually reported in mV/s) is a very important parameter because it is inversely proportional to the intensity of the current peaks. It is usually kept constant throughout the whole experiment. The current is plotted against the voltage and the graph obtained is called a cyclic voltammogram (figure 2.5.2).

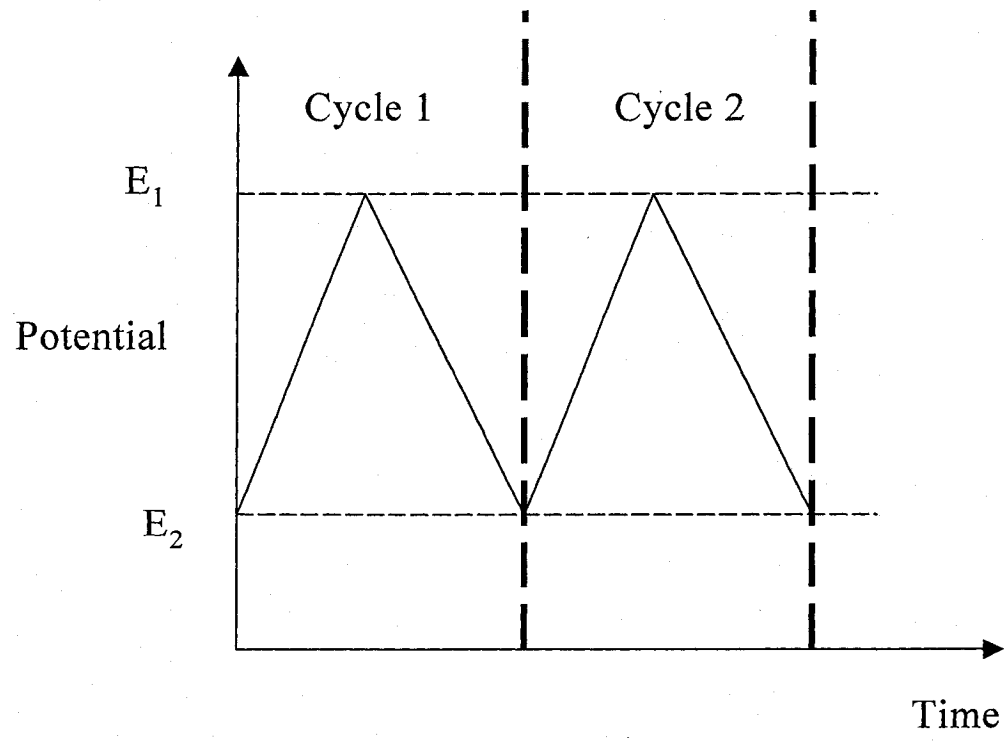

Figure 2.5.1: Potential variation in a typical CV experiment. Two cycles are shown.

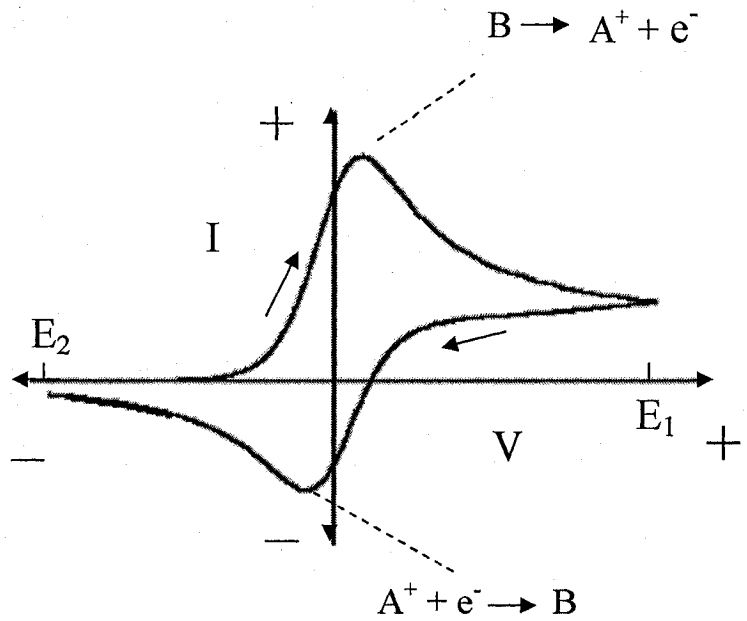

Figure 2.5.2: Cyclic voltammogram of a reversible redox couple: A^+/B. One cycle is shown. The arrows indicate the direction of the scan.

In figure 2.5.2, a redox couple A^+/B is placed in an electrochemical cell and a CV experiment is conducted. First the voltage is scanned in the negative direction (right to left), which means that electrons are being injected into the cell and so A^+ is being reduced into B. This will go on until all the A^+ species at the surface of the working electrode are reduced. A minimum is thus reached and a reduction peak is formed.

When the potential reaches E_2, the scan direction is reversed (from left to right). Electrons are now being withdrawn from the cell. The current starts to increase positively and B is being oxidized back into A^+. This will go on until all the B species at the surface of the working electrode are oxidized and thus an oxidation peak is formed. Then the current decreases again until the scan is stopped back at E_1 (29).

Chapter 3:

Materials and Methods

3.1. Reagents

Table 3.1.1 lists the chemical reagents used throughout this project. Aqueous solutions were prepared with distilled-deionised water. The glucokinase, the N-(5-amino-1-carboxypentyl) iminodiacetic acid (NTA ligand), the glutaraldehyde, the 4-nitrobenzenediazonium tetrafluoroborate salt, and 1-Ethyl-3-(3-dimethylaminopropyl)-carbodiimide (EDC) were stored at a temperature of 5 °C. The rest of the reagents were stored at room temperature.

Table 3.1.1: Reagents used.

Reagent	Supplier	Purity
Tricholorethylene	Fisher	Reagent Grade
Acetone	Fisher	Reagent Grade
Methanol	Fisher	Reagent Grade
Ethyl Alcohol	Sigma-Aldrich	HPLC grade
Hydrofluoric Acid (48 – 50 %)	Fisher	48 – 50 %
Sulfuric Acid	J.T. Baker	Reagent Grade
Hydrochloric Acid	Fisher	36.5 – 38.5 %
Ammonium fluoride (40 %)	J.T. Baker	Electronic grade, Low Sodium MOS.
Glutaraledhyde	Sigma	25% solution
4-Nitrobenzeneidazonium Tetrafluoroborate	Aldrich	97 %
Sodium Chloride	Fisher	Reagent Grade
Potassium Chloride	Fisher	Reagent Grade

NTA Ligand	Qiagen Inc.	Reagent Grade
Nickel (II) Chloride hexahydrate	Sigma - Aldrich	Reagent Grade
β-D(+)Glucose	Sigma	97 %
Phosphate Buffered Saline Tablets	Sigma	Reagent Grade
Tris Buffered Saline Tablets	Sigma	Reagent Grade
EDC	Sigma	Reagent Grade
Calcium Carbonate	Sigma	Reagent Grade
Glucokinase and non-specific protein	Lady Davis Institute	
Nitrogen gas	PraxAir	UHP

3.2. Electrodes and experimental set-ups.

3.2.1. n-type Semiconductor Silicon Electrodes.

These electrodes were purchased from Silicon Valley Microelectronics Inc. They were phosphorous doped with a density of 10^{15} atoms/cm^3. Figure 3.2.1.1 is a schematic diagram of these substrates, which are 1cm x 1cm chips taken from diced 10cm diameter wafers. Chromium/gold layers were evaporated onto the back of the silicon substrate to ensure ohmic contact. Both Si(100) and Si(111) crystal orientations were used.

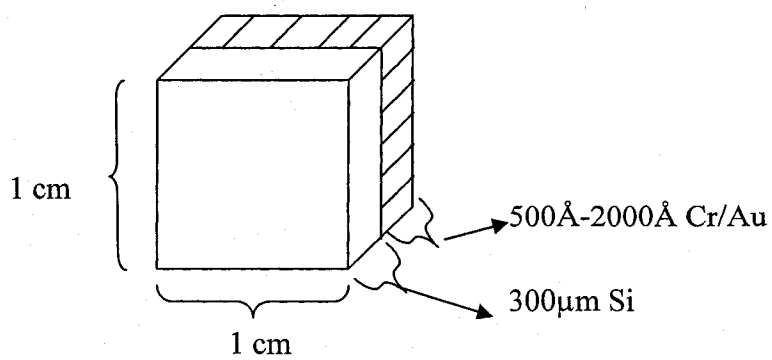

Figure 3.2.1.1: Silicon substrates.

In order to functionalize and realise impedance measurements, these silicon chips were used as working electrodes in a three-electrode set-up (figure 3.2.1.2).

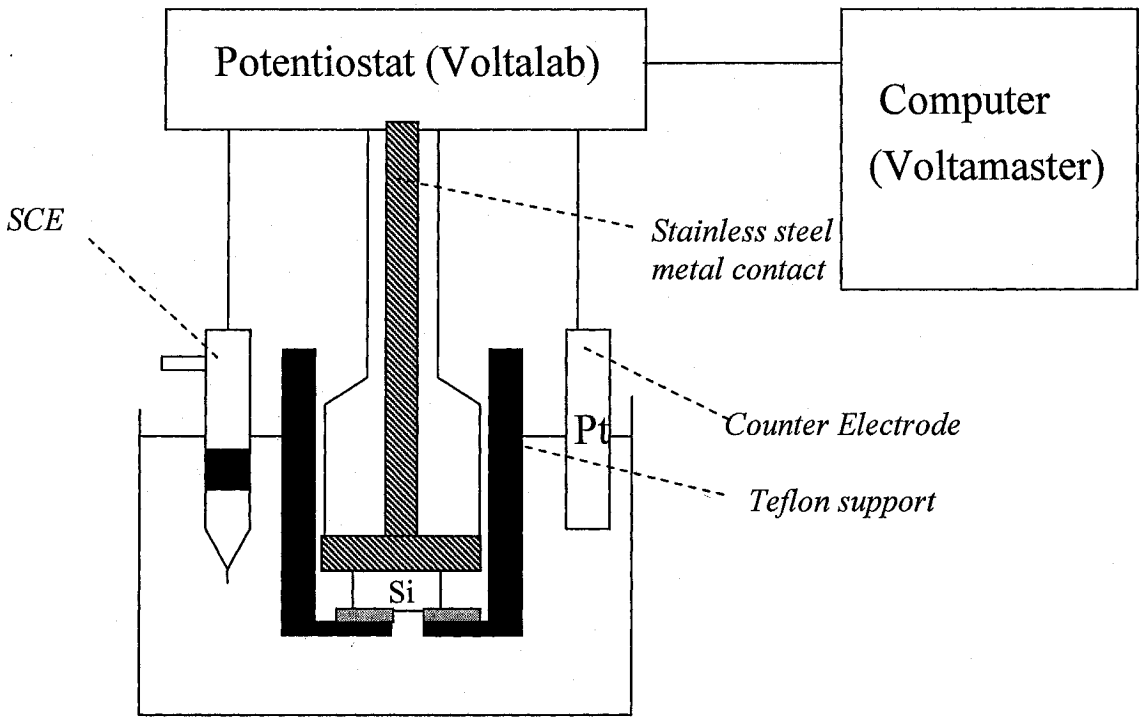

Figure 3.2.1.2: Experimental set-up used with the Si chips.

In figure 3.2.1.2, the reference electrode is a mini saturated calomel electrode purchased from Fisher Scientific (Accumet Electrode). The counter electrode is a platinum foil (from Alfa Aesar) and the silicon chip is the working electrode. The current flows between the working and the counter electrodes, whereas the potential of the working electrode is measured against the reference electrode (22). Approximately 15mL of electrolyte were used with this cell. In the case of impedance measurements, the whole set-up was put in a dark box, to avoid any interference from photocurrents.

All three electrodes were connected to a source: Voltalab PGZ 301 potentiostat. The latter was controlled by a computer program: Voltamaster 4, version 3.0.

The platinum foil had to be cleaned regularly. This was done by dipping it in a solution of saturated potassium dichromate and sulphuric acid (5:95, v/v), during 20 minutes. The electrode was then thoroughly washed with methanol, and left to dry.

3.2.2 Screen Printed Carbon electrodes (SPEs).

Figure 3.2.2.1 is a picture of an SPE. They are composed of 8 working electrodes (labelled WE), one central disk-shaped counter electrode (labelled CE) and one ring-shaped pseudo-reference electrode (labelled Ref). Each working electrode can be addressed individually.

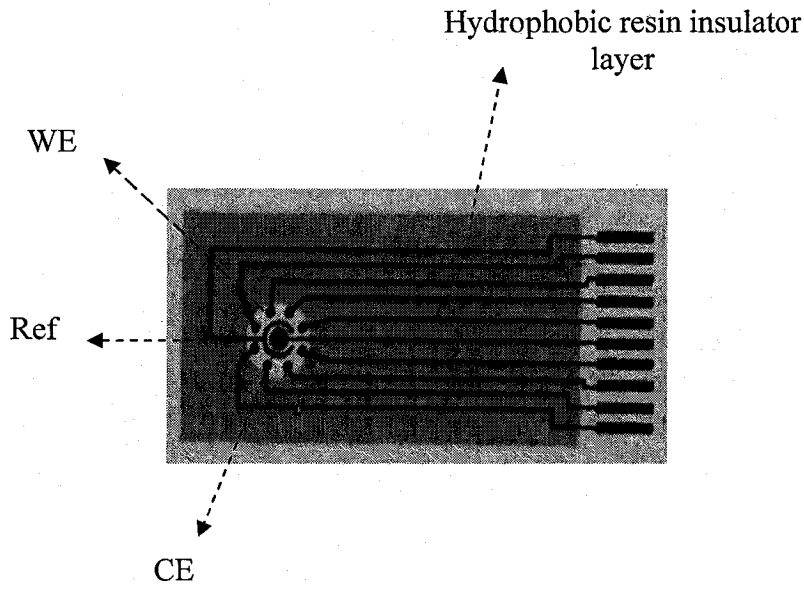

Figure 3.2.2.1: SPE electrode (10 mm x 25 mm). Each WE has a surface of 780 μm^2.

These network electrodes were prepared using a previously published method. "The screen-printing machine was a DEK 248. A polyester monofilament fiber screen with a mesh size of 260 counts/in and a thickness of 13 μm was used to print the carbon ink (Electrodag 423 SS; Acheson) onto an A5 (21 cm x 14.8 cm) polyester flexible foil. After printing, the polyester foils supporting 16 electrode arrays were baked 10 minutes at 100°C to cure the thermoplastic carbon ink. A second layer, composed of insulating polymer (Minico M 7000; Acheson) was then printed on the networks to define a window delimiting the active area of the electrode." (28)

These SPEs present several advantages over their Si counterparts:

- They are robust, very low cost and disposable.
- Their pattern can be easily changed.
- They are user-friendlier because their experimental set-up is much simpler: the SPE is inserted into a connector that relates it to the potentiostat through ten electrical wires. This connector was taken from a CD player (figure 3.2.2.2). 50μL of solution were deposited onto the electrodes. The resin renders the surface hydrophobic, which prevents the electrolyte from spreading. The same set-up was used for the electrode modifications, as well as for the impedance measurements.

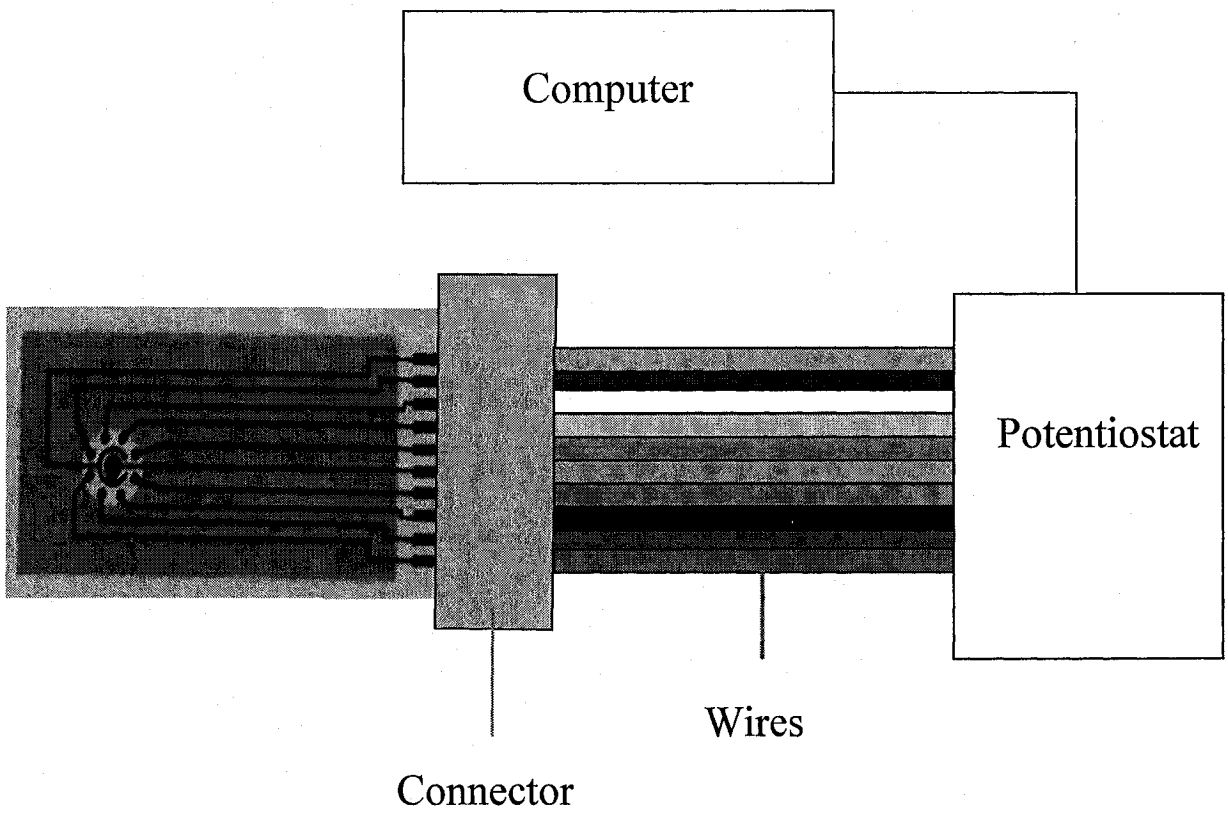

Figure 3.2.2.2: Experimental set-up used with the SPEs.

3.3. Preparation of the biosensor.

The most crucial step in the development of our biosensor is the immobilization of the glucokinase (30, 31). Indeed, the immobilization procedure had to allow for it to keep its glucose binding ability, once it was attached to the electrode.

There is a wide range of techniques for enzyme immobilization onto bio-specific surfaces. Adsorption is the easiest and the most widely used method for this purpose. The enzyme is immobilized onto a solid support (e.g: glass, silica, diatomaceous earth, ion exchange resins, biopolymers, SPEs..etc) through low energy binding forces (Van der Waals interactions, hydrophobic forces, hydrogen bonds, ionic bonds..etc). Enzymes can also be immobilized through entrapment within a polymeric cage (e.g: electropolymers, polyvinyl imidazole cross-linked with polyethylene glycol diglycidyl ether, sol-gels....etc). The major drawback of these non-covalent techniques is that the weak bonds between the enzyme and the matrices do not yield stable biosensors. Consequently, they suffer from severe leakages of the bio-molecule as well as degradation of performance with use (32, 33).

In the literature, covalent coupling is considered the best approach for biosensor preparation. These procedures usually go through activation of the matrices in order to obtain functionalities that will subsequently react with the enzyme (examples: cyanogen bromide, carbonydiimidazole, water soluble carbodiimides, bifunctional cross-linking agents such as glutaraldehyde...etc) (45).

During this work, different covalent immobilization schemes were explored in order to find the one that will keep the activity of the enzyme after its coupling to the electrode. The following are the experimental procedures used for each one.

3.3.1. Enzyme immobilization using 4-nitrobenzenediazonium salt and glutaraldehyde.

This method was used with both types of electrodes (Si and SPE). Figure 3.3.1.1 is a summary of the various steps used with the Si electrodes. The procedure is the same with the SPEs, except that there is no etching step. Indeed, in order to obtain H-terminated Si chips, these electrodes have to be etched prior to functionalization.

The etching started with the cleaning of the electrodes. They were first dipped, during 1 minute, in a flask containing 15 mL of trichloroethylene. Then they were transferred into a flask containing 15 mL of acetone, for 1 minute. Finally, they were immersed in a third flask containing 15 mL of methanol, for 1minute. The etching then proceeded by dipping the electrode in 15 mL of HF (50%) and then transferring them into a flask containing 15 mL of ammonium fluoride (40%), for 6 minutes. The chips were then washed with d-d water for 30s. Finally, they were dried in a stream of gaseous nitrogen (9).

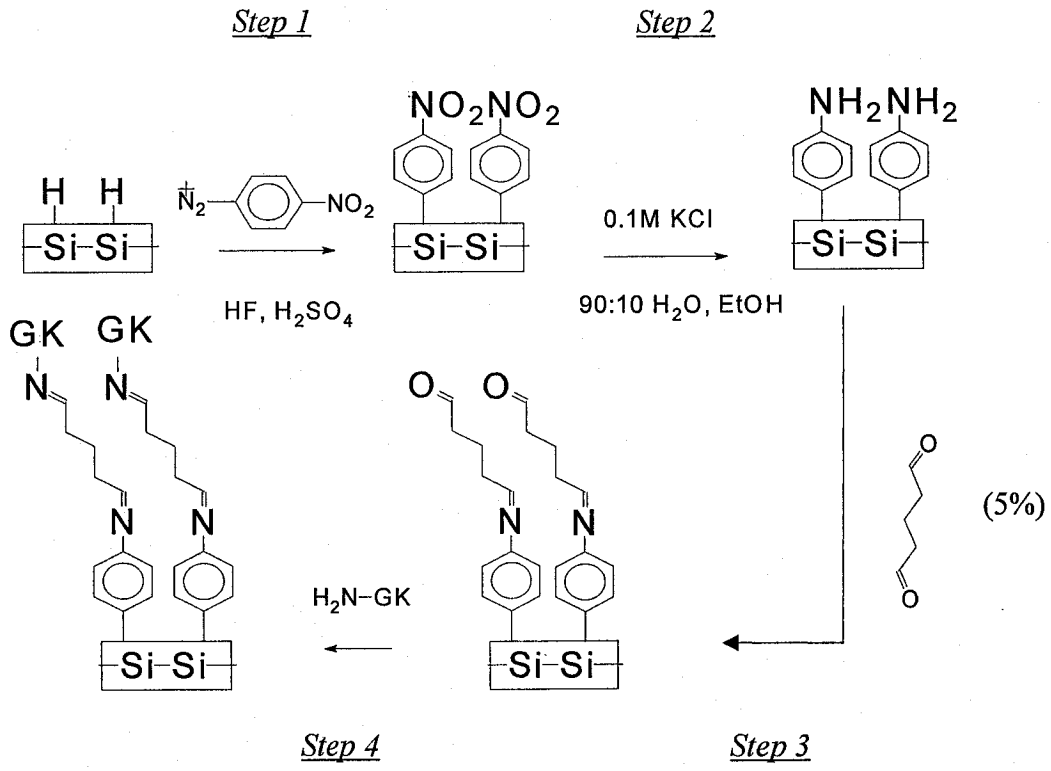

Figure 3.3.1.1: Preparation of the biosensor using nitrobenzene diazonium and glutaraldehyde.

After the etching, the chips were put in the set-up of figure 3.2.1.2 in order to functionalize them (figure 3.3.1.1, step 1). This was done by reducing the nitrobenzene diazonium onto the surface of the chip, using cyclic voltammetry (potential range: -0.6V to -1.7V. Scan rate: 20 mV/s). The electrolyte was a freshly prepared aqueous solution of nitrobenzene diazonium tetrafluoroborate, 2 mM, sulfuric acid, 0.1M, and HF, 2% (v/v). This solution was then degassed by bubbling nitrogen for about 20 minutes.

In the second step, the nitro group of the sensor is reduced to an amine group. This was also done using cyclic voltammetry, where the electrolyte was a solution of KCl (0.1M) dissolved in a 90:10 (v/v) water/ethanol mixture. The potential range was from –0.4V to –1.6V at a scan rate of 100 mV/s (32, 33).

The chip was further modified with glutaraldehyde (step 3, figure 3.3.1.1). This was done by dipping it in a test tube containing 1mL of a 5% (v/v) aqueous solution of glutaraldehyde. The electrode was allowed to react for 30 minutes at room temperature (9).

The fourth and final step is the enzyme immobilization. The chips were put in a petri-dish containing a moistened kimwipe paper. 50μL of the enzyme solution was deposited onto the chip and left to react for 1h. The amine groups of the glucokinase were expected to react with the aldehyde moiety of the surface glutaraldehyde. The chips were now ready to be put in contact with a solution of glucose.

The electrodes were washed with d-d water for 30s and dried under nitrogen, after each modification step.

3.3.2 Enzyme immobilization using NTA ligand: in-situ generation of diazoniums.

This method was inspired from a well-known protein separation technique: ion metal chelating affinity chromatography (IMAC) (34-36, 39-42). Qiagen Inc, a leader in this field, developed and commercialized chromatography nickel beads by loading the NTA ligand shown in figure 3.3.2.1 with nickel ions, and covalently attaching it onto aragose beads (figure 3.3.2.2). The proteins in solution are eluted onto the beads and only the ones bearing a histidine tag are able to coordinate to the nickel ion and are thus separated from the rest. We have attempted coupling this NTA ligand onto our electrodes (43).

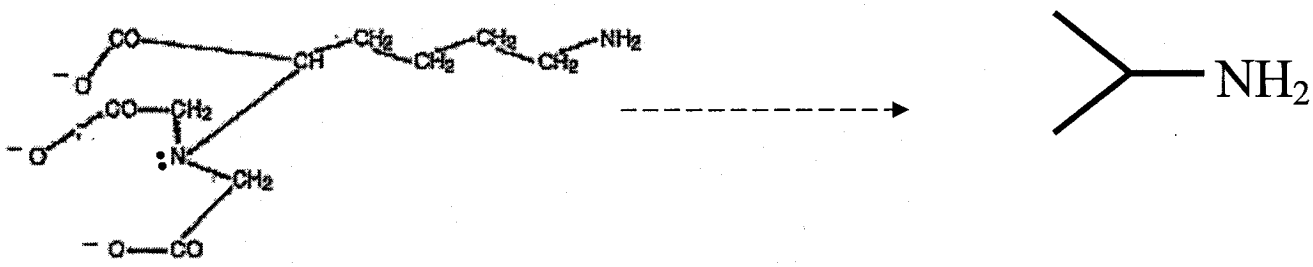

Figure 3.3.2.1: Structure of the NTA ligand that was coupled to the electrodes (left), and ligand simplified representation (right).

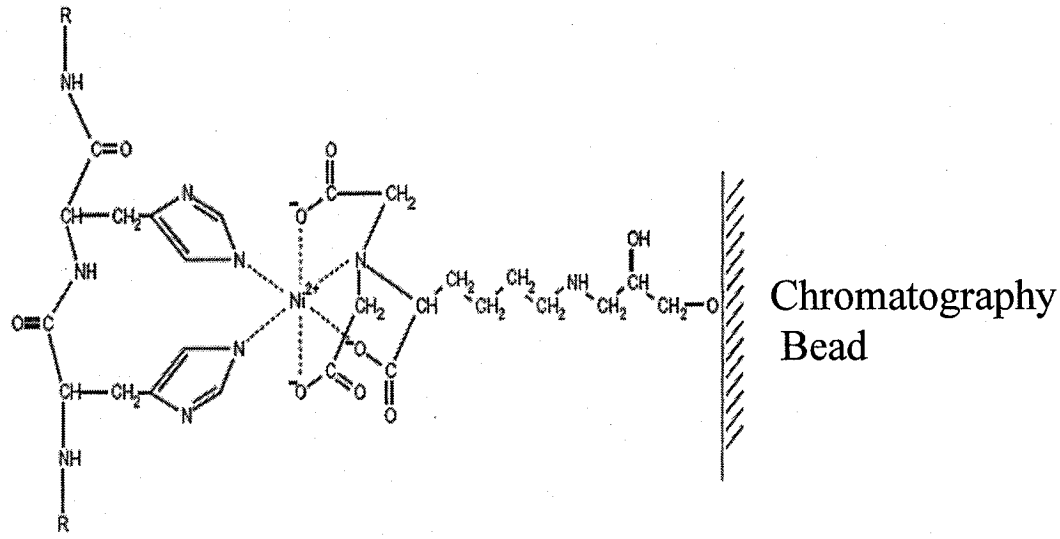

Figure 3.3.2.2: Chelating affinity between the histidine-tagged enzyme and the Qiagen chromatography bead (43).

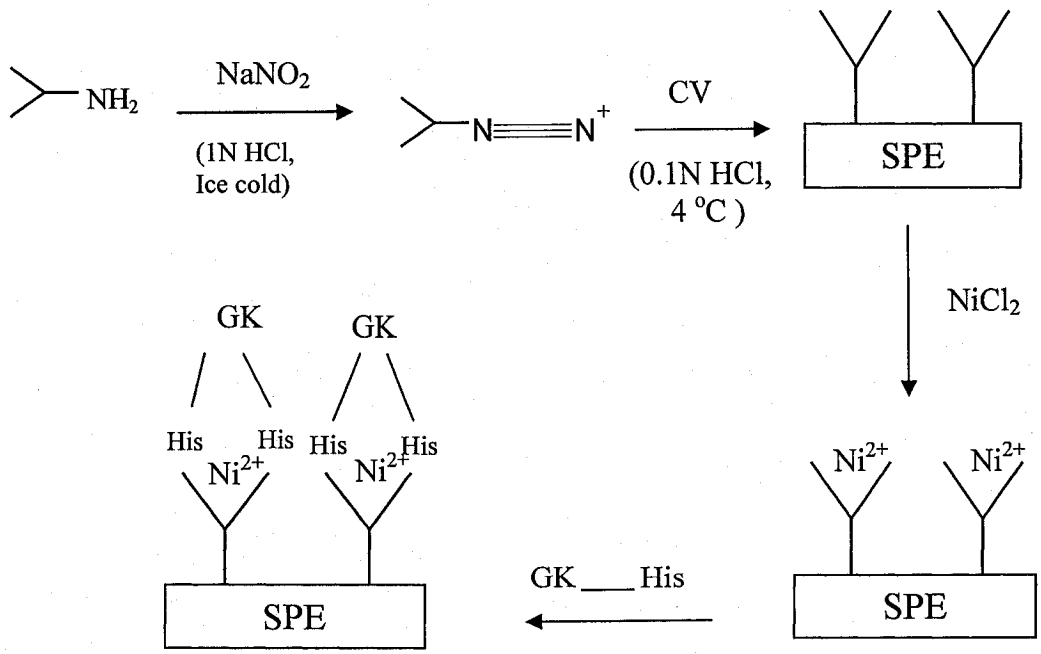

Figure 3.3.2.3: Various steps for enzyme immobilization using NTA ligand, through in-situ generation of diazoniums.

Figure 3.3.2.3 is a flowchart of the experimental procedure used on the functionalization of an SPE electrode. The first step is the in-situ generation of diazoniums. 44 μL of an ice-cold solution of sodium nitrite (7.6 mg/mL) in water was combined with 1 mL of an ice-cold solution of the NTA ligand (1 mg/mL) in 1N HCl (de-aired with nitrogen for 20 minutes). They were left to react for about 5 minutes. They were then combined with 1mL of 0.1N HCl (ice cold, degassed with nitrogen for 20 minutes) and 50μL of this solution was deposited onto the SPE. A CV (voltage range: -0.7 V to –1.7 V at 20m V/s) was run in order to modify the electrode. The diazonium moiety is now reduced and the ligand covalently attached onto the electrode.

The next step is the loading with nickel ions. A 1 mM solution of $NiCl_2$ in phosphate buffer was prepared. 50μL were deposited onto the SPE for 30 minutes. Finally, 50 μL of the 6-histidine tagged glucokinase were deposited onto the SPE for 1h. The electrode was carefully rinsed with d-d water and dried under nitrogen, after each step (44).

In the case of the Si electrodes, the procedure was mostly the same. A smaller volume of electrolyte had to be used (maximum volume: 5mL), and so the Teflon cover in figure 3.2.1.2 was too big for this new considerably smaller cell. The set up had to be changed, the back of the silicon chip was thus covered with an insulating piece of tape and then it was simply dipped into the electrolyte (figure 3.3.2.4).

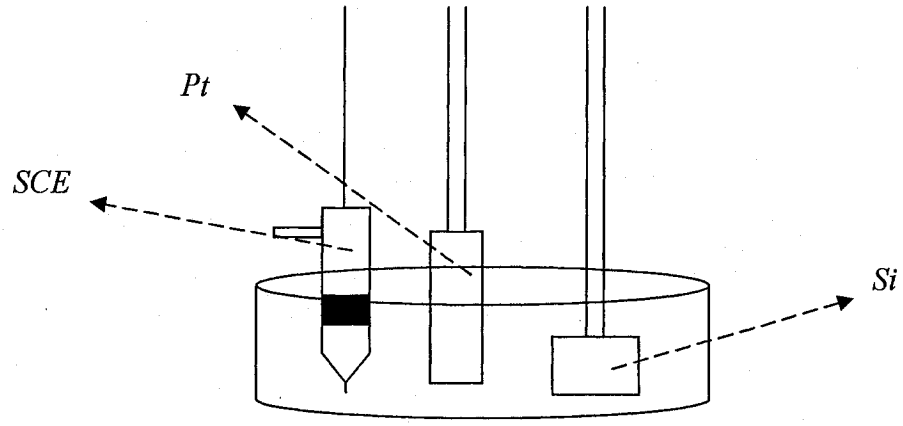

Figure 3.3.2.4: Set-up used with Si electrodes for the CV run of figure 3.3.2.4 (volume: 5mL).

3.3.3 Preparation of the biosensor using NTA ligand and EDC.

In this method, the NTA ligand was coupled to the electrodes (SPEs only) after their activation with 1-Ethyl-3-(3-dimethylaminopropyl)-carbodiimide (EDC, figure 3.3.3.1). A potential of +2.2 V was applied for 10 minutes with a solution of EDC in 0.12N HCl as the electrolyte (28). The latter was previously nitrogen-bubbled for 20 minutes. An activated ester intermediate is formed. The electrode was then carefully washed with d-d water and 50 µL of a solution of the NTA ligand in $CaCO_3$ (0.1M, pH = 11), was deposited for 30 minutes. The ligand is thus covalently attached to the SPE, and a water-soluble by-product, O-acyloisourea, is formed. The metal loading and the enzyme immobilization were done as described previously (section 3.3.2).

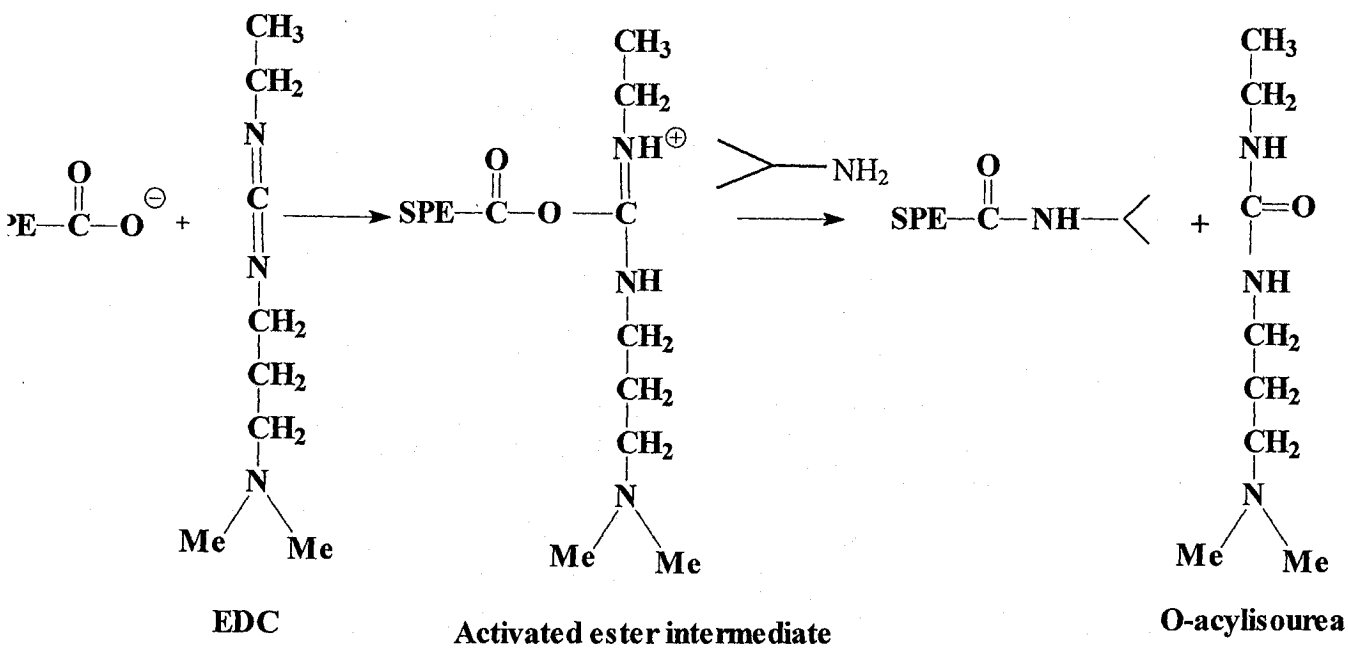

Figure 3.3.3.1: Coupling of the NTA ligand to the SPE using EDC activation (45).

3.4. Enzyme activity measurements.

We have attempted to evaluate the activity of the immobilized glucokinase using standard methods. The following is a brief description of the procedure. In a test tube, the electrode with the immobilized glucokinase, is put in contact with a solution of glucose, adenosine triphoshphate (ATP) and Mg^{2+}. If the enzyme is active, it should catalyze the phosphorylation of glucose into glucose-6-phosphate (G6P, figure 3.4.1). If $NADP^+$ is later on added with G6P dehydrogenase, 6-phosphoglucono-δ-lactone and NADPH are produced. The latter can be detected using UV absorbance. Thus aliquots of the mixture are taken at different times, and their absorbance (at λ = 340 nm) is measured as the reaction progresses.

$$\text{Glucose} + \text{ATP} \xrightarrow[Mg^{2+}]{GK} \text{G6P} + \text{ADP}$$

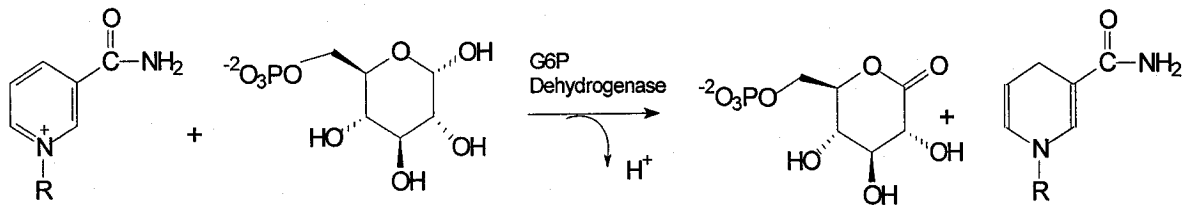

$NADP^+$ G6P 6-Phospholglucon-δ-lactone NADPH

Figure 3.4.1: Reactions involved in the enzyme activity test (14, 46).

Chapter 4:

Results and Discussion

4.1. Enzyme immobilization through electrode modification with nitrobenzene diazonium and glutaraldehyde.

4.1.1. Silicon chips as substrates.

This method was inspired from a protocol previously developed in our laboratory, which was intended for single DNA strands immobilization (9, 21). Consequently, it was the first method used for enzyme immobilization. As described in the experimental section, the Si substrate is first etched then modified with nitrobenzene diazonium using cyclic voltammetry (refer to step 1 of figure 3.3.1.1).

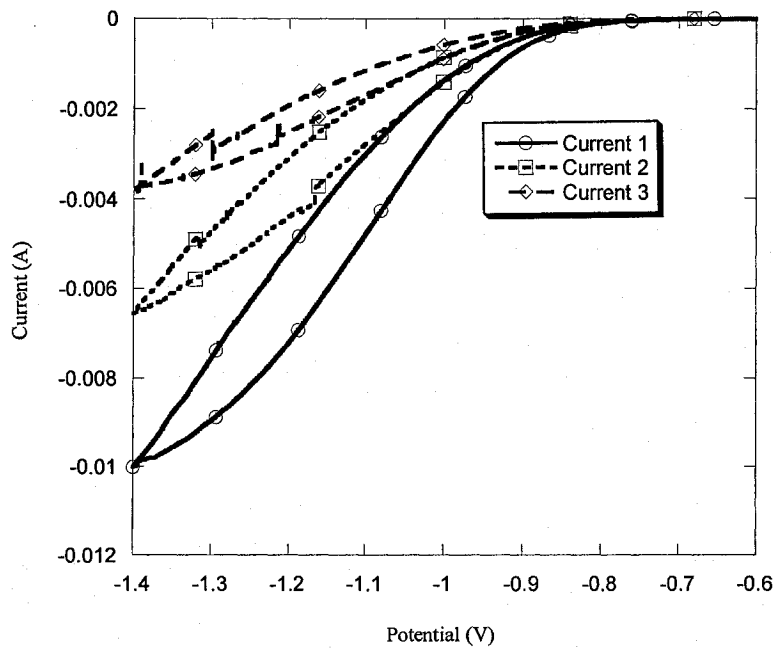

Figure 4.1.1.1: Cyclic voltammogram for Si modification with $NO_2ArN_2^+$. Scan rate: 20 mV/s.

Figure 4.1.1.1 shows a typical cyclic voltammogram obtained for this step. Three scans were run from –0.4 V to –1.4 V (vs SCE) at a scan rate of 20 mV/s in order to allow the electroactive species to react sufficiently (23). In the first scan (labeled "current 1"), the current starts to increase negatively at around -0.8V and an irreversible reduction wave is recorded. The current's intensity reaches –0.01 A, which is considered a high current showing good reactivity between the nitrobenzene diazonium and the chip. The intensity decreases with the second and third scans, which was to be expected since there are fewer and fewer reduction sites available to the nitroarlydiazonium. The electrode is gradually being pacified.

The next step was the reduction of the aniline moiety into an amine (step 2 of figure 3.3.1.1).

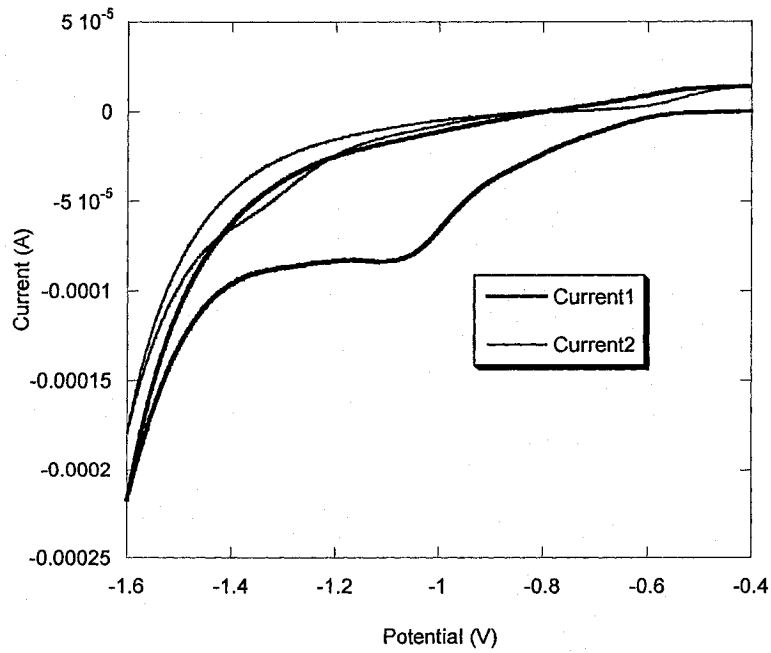

Figure 4.1.1.2: Cyclic voltammogram obtained for the reduction of NO_2Ar into NH_2Ar. Scan rate: 100 mV/s.

Figure 4.1.1.2 shows a typical voltammogram after this step. In the first scan, an irreversible reduction wave centered at about –1.07 V (vs SCE) is recorded. It practically disappears on the second scan.

The surface modifications were monitored using impedance Mott-Schottky measurements (figure 4.1.1.3).

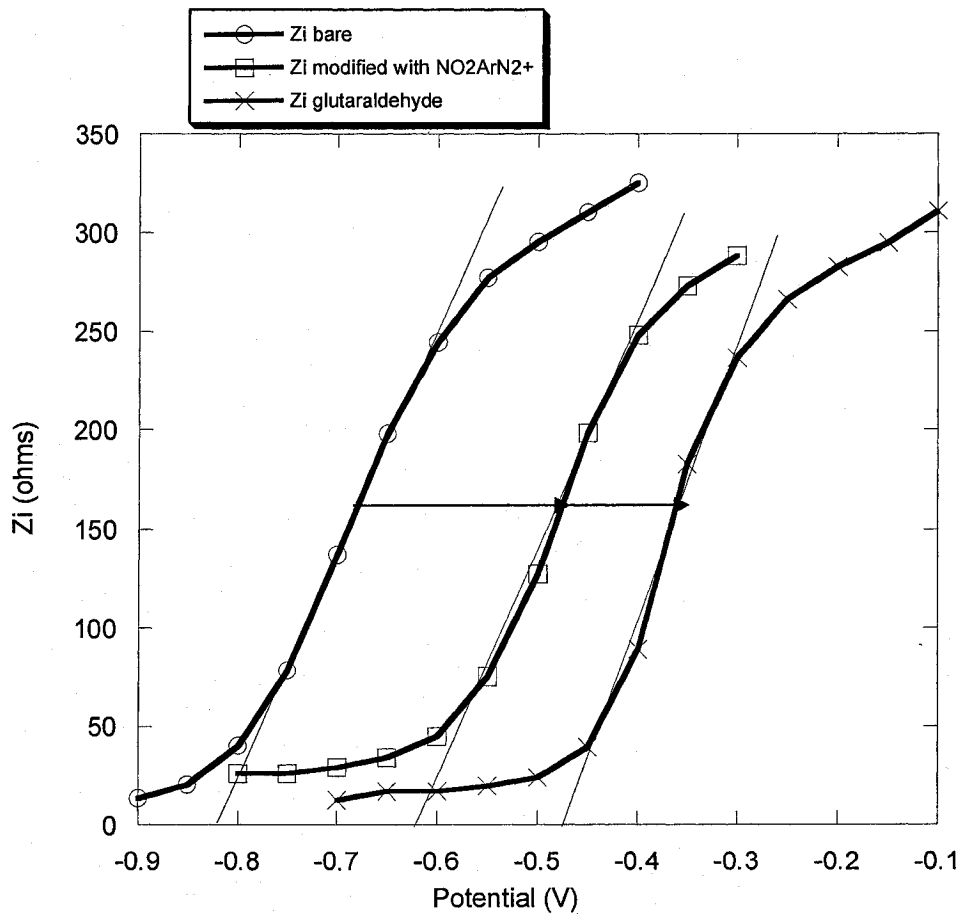

Figure 4.1.1.3: Impedance measurements of the Si electrode modified with nitrobenzene diazonium and glutaraldehyde.

In figure 4.1.1.3, the slope of each curve in the depletion region was extrapolated in order to evaluate its flat band potential (V_{fb}, intersection between the straight line and the x axis). The surface modifications are seen to cause significant shifts in the V_{fb}. A positive shift of + 0.202V between the etched chip (labeled "bare") and after its modification with nitrobenzene diazonium and reduction of the NO_2 moiety into NH_2. After the glutaraldehyde treatment, another significant positive V_{fb} shift of +0.147 V was recorded. The glucokinase was then immobilized onto the electrode and impedance measurements were taken at an initial concentration of 5 µg/mL. (figure 4.1.1.4).

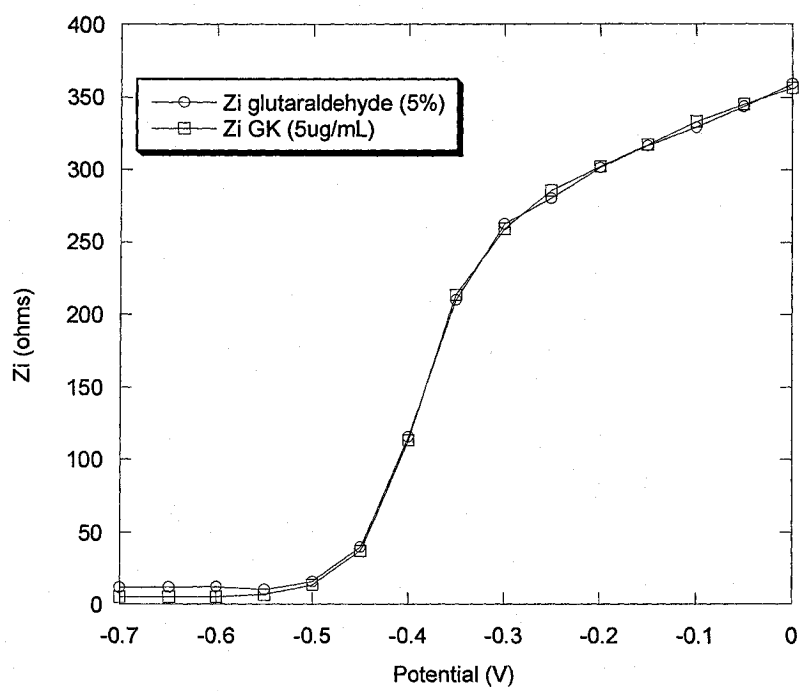

Figure 4.1.1.4: Mott-Schottky curves for an Si chip modified with glutaraldehyde and GK 5µg/mL (in Tris HCl buffer, pH 7.4).

As shown in figure 4.1.1.4, no V_{fb} shift could be detected under these conditions. This may indicate that the glucokinase was not immobilized, or that the concentration used was insufficient. Thus, measurements were performed at a higher concentration of 25 µg/mL and figure 4.1.1.5 shows the resulting Mott-Schottky curves.

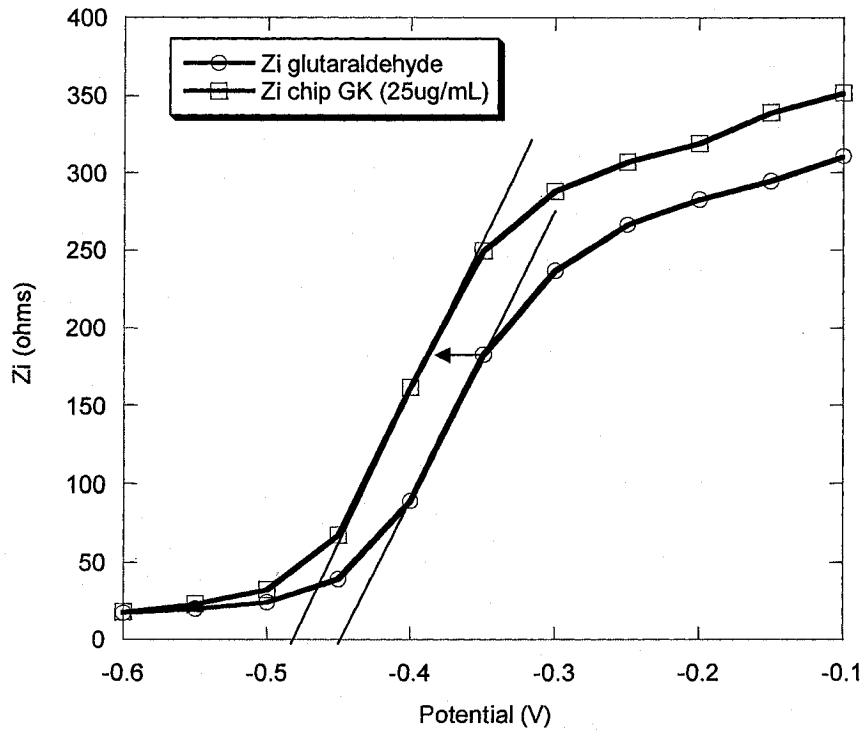

Figure 4.1.1.5: Mott-Schottky curves for an Si chip modified with glutaraldehyde and GK 25µg/mL.

A significant V_{fb} negative shift of –0.042 V is now observed after the deposition of the glucokinase. To verify that this shift was indeed due to the enzyme, a control experiment was run where only the buffer in which the GK was diluted (Tris HCl, pH = 7.4) was

deposited onto the chip for 1h. Figure 4.1.1.6 shows that no V_{fb} shift occurred, confirming the previous result.

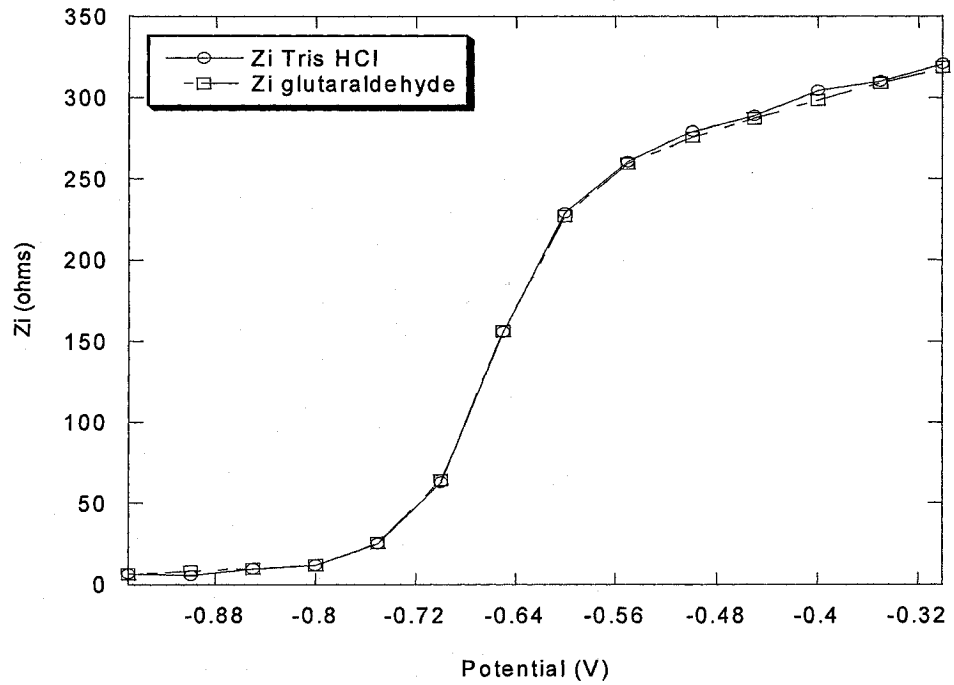

Figure 4.1.1.6: Control experiment for the enzyme immobilization.

These electrodes were now ready to be tested in the presence of glucose. The latter was prepared in Tris HCl buffer as well. The set up in figure 3.2.1.2 was placed onto a magnetic stirrer, and a stirring bar was added to the cell. Figure 4.1.1.7 shows the resulting Mott- Schottky curves when a concentration of 8mM of glucose was used (blood glucose concentration range of a diabetic person: 5 – 8 mM).

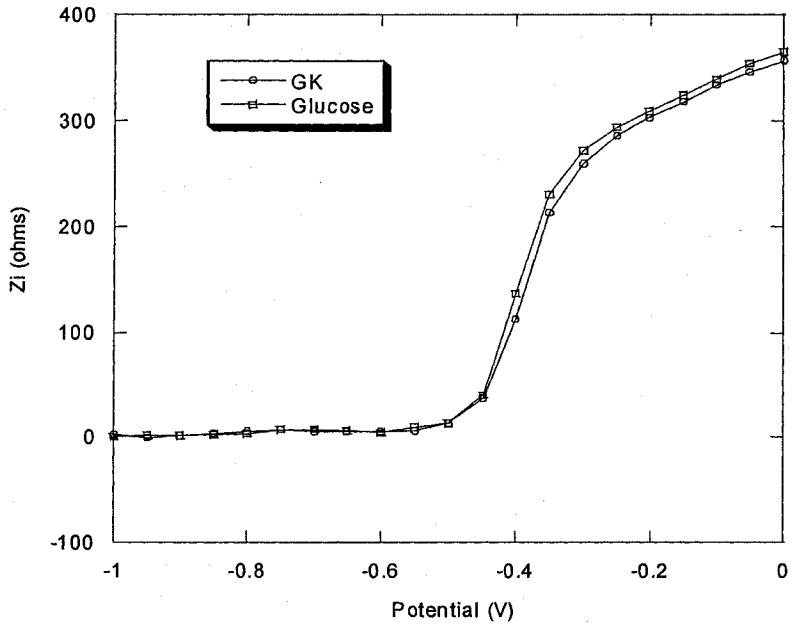

Figure 4.1.1.7: Impedance curves for glucokinase and glucose (8 mM).

There was no significant shift between the glucokinase curve and the glucose curve. This was probably due to two reasons: either the glucose did not bind to the enzyme or not enough glucose was present to produce an observable V_{fb} shift. Again, an increase in concentration to 100 mM of glucose was tested (figure 4.1.1.8).

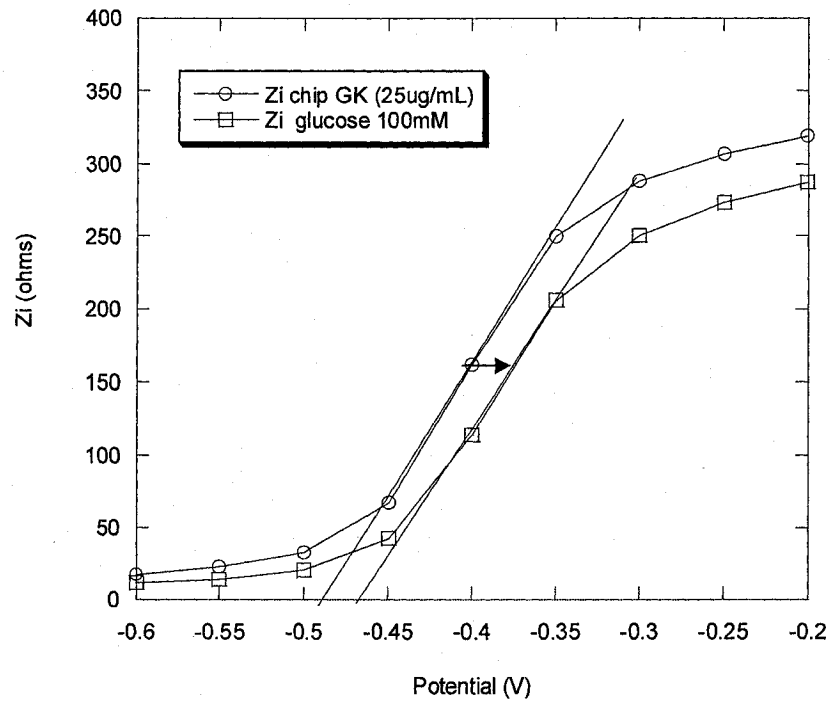

Figure 4.1.1.8: Impedance curves for GK and glucose (100 mM).

As shown in figure 4.1.1.8, there is now a positive V_{fb} shift of +0.030 V, when glucose is added to the electrolyte.

4.1.2. Immobilization of a glucose non-specific protein.

To demonstrate the fact that the glucose is not necessarily binding to the active site of the enzyme, an attempt was made at modifying the Si electrode with a glucose non-specific protein solution. Figure 4.1.2.1 shows the resulting Mott-Schottky curves.

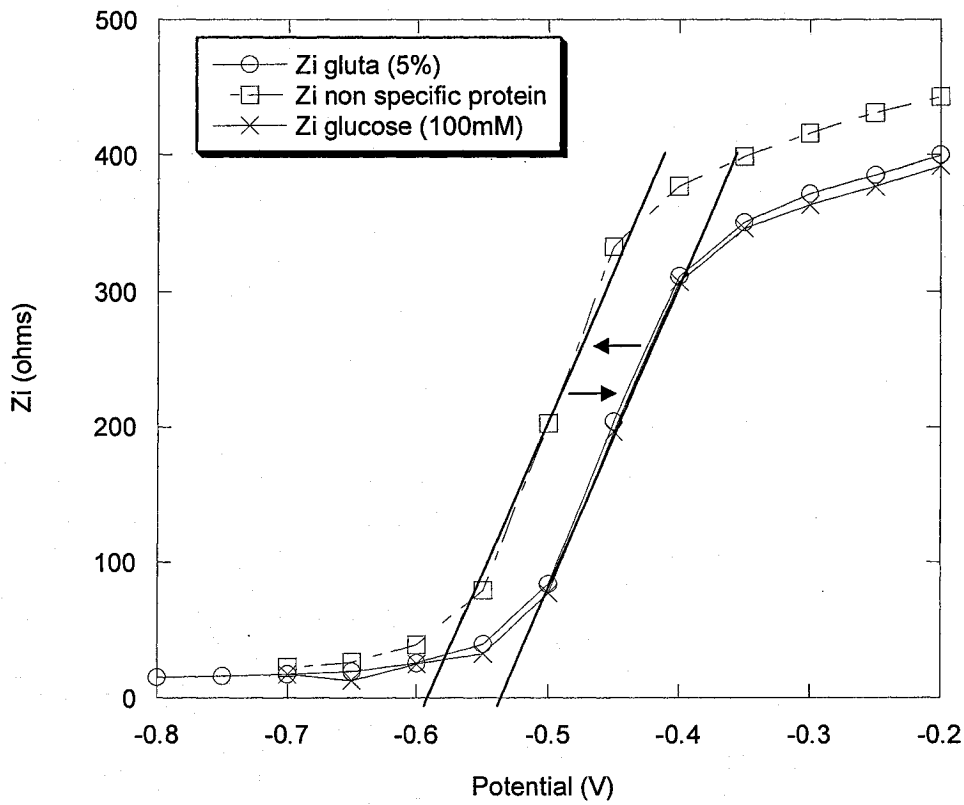

Figure 4.1.2.1: Immobilization of a non-glucose specific protein ("gluta" stands for glutaraldehyde)

When this protein is immobilized, it causes a negative shift of –0.045 V. When it is put in contact with a solution of glucose, a positive shift of +0.045 V is observed. These shifts are of the same magnitude and algebraic sign as when the glucokinase was immobilized. These results reinforce the hypothesis that the glucokinase is randomly attached to the electrode and the shifts that were observed could be due to specific, as well as non-specific, adsorption of the glucose to the surface.

4.1.3. SPEs as substrates.

The functionalization approach used for Si chips was also tested on screen-printed carbon electrodes (SPEs). As stated in section 3.2.2, these electrodes present several advantages over the silicon ones.

The first step was their modification with nitrobenzene diazonium and then the reduction of the nitro goups to amino groups. Figures 4.1.3.1 and 4.1.3.2 show the resulting cyclic voltammograms when only two of the eight working electrodes were addressed.

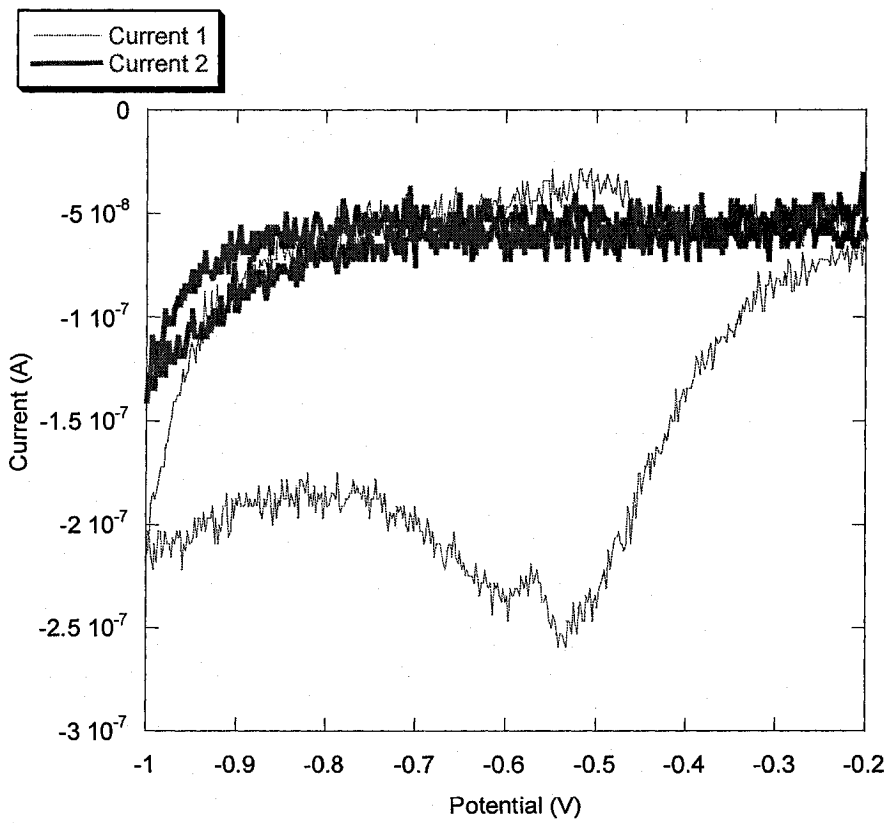

Figure 4.1.3.1: Cyclic voltammogram for the modification of an SPE with nitrobenzene diazonium. Scan rate: 200 mV/s

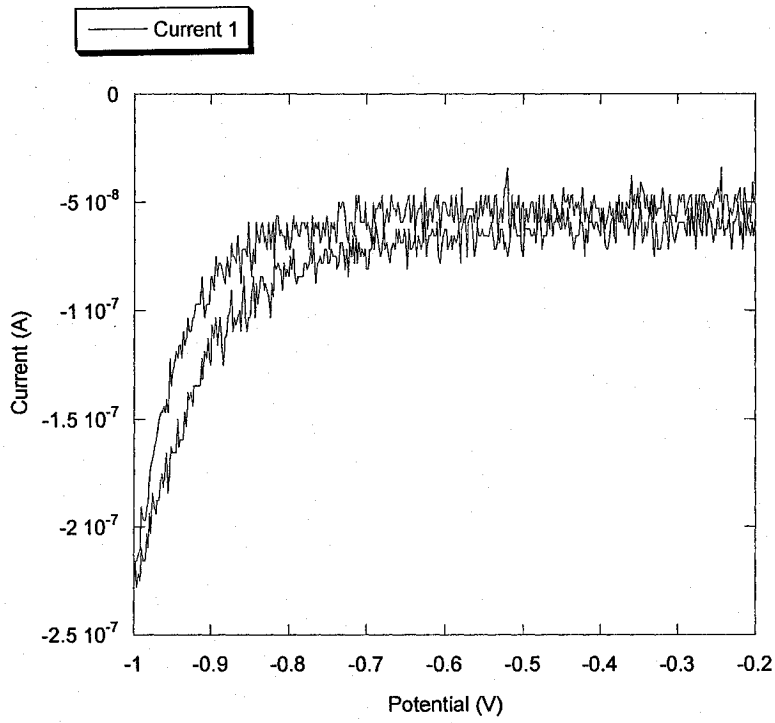

Figure 4.1.3.2: Cyclic voltammogram for the reduction of nitro groups to amino groups. Scan rate: 200 mV/s.

In figure 4.1.3.1, two scans were run from –0.2 V to –1.0 V. In the first one, a significant reduction wave, centered at about –0.55 V was recorded. This shows good reactivity between the electrolyte and the surface of the SPE. In the second scan, the wave practically disappears. These results are very similar to the ones obtained with the Si electrodes. In figure 4.1.3.2, where the NO_2 groups are reduced to NH_2, only one scan is shown. Despite the noise, a reduction wave can be seen starting at about –0.7 V. Once again, these results are consistent with the ones obtained with the Si chips.

These voltammograms are much noisier than the ones observed when using the Si electrodes because of the small surface area that the SPEs present. Indeed, the latter have a surface area of 1560 μm^2 or 1.56×10^{-3} mm^2 (for 2 working electrodes of the SPE

network), whereas the Si electrodes offer a working surface of ~ 78 mm^2. These electrochemically functionalized SPEs were then submitted to the same glutaraldehyde treatment used for the Si electrodes.

Impedance measurements were again used to monitor these modifications, but as stated in chapter 2, impedance variations using conducting electrodes such as the SPEs, are monitored through Nyquist plots rather than Mott-Schottky plots (Figure 4.1.3.3).

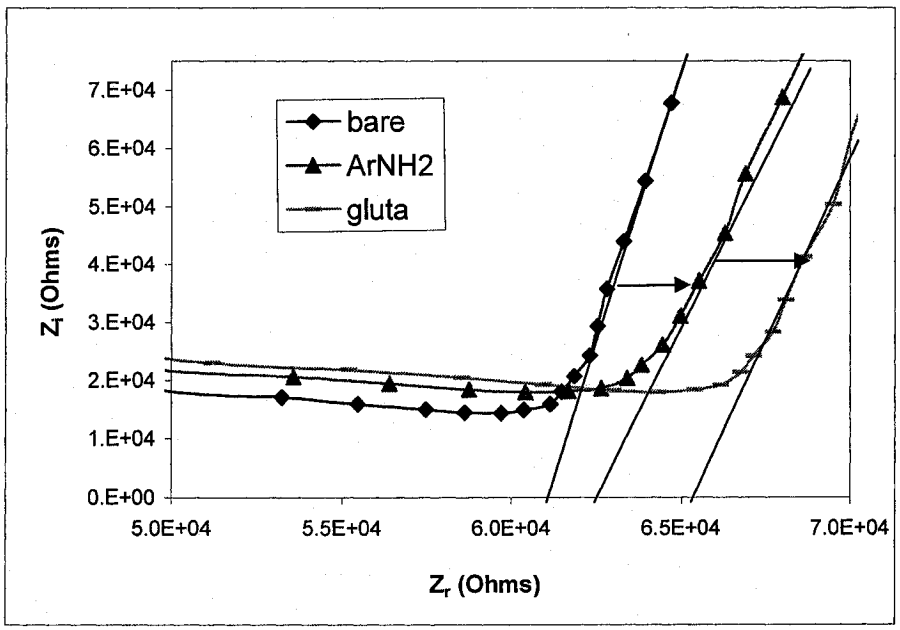

Figure 4.1.3.3: Nyquist plots for the modification of an SPE with nitrobenzene diazonium and glutaraldehyde (labeled "gluta").

In figure 4.1.3.3, three Nyquist plots are shown, where the linear regions at low frequencies for each plot were extrapolated to the x-axis, in order to evaluate the term: $R_\Omega + R_{ct} - 2\sigma^2 C_d$ (refer to chapter 2, figure 2.4.3). Recall that this term is directly related to the capacitance of the double layer at the surface of the electrode.

A significant positive shift of ~ $1.1x10^3$ Ω is observed between the extrapolated value obtained from the curve of the bare SPE and that obtained for the curve corresponding to nitrobenzene attachment followed by reduction of the nitro to amino groups. Another significant positive shift of ~ $3.4x10^3$ Ω, is observed after the glutaraldehyde treatment. The next steps involve the immobilization of the glucokinase and the glucose detection. The Nyquist plots for these are shown in Figure 4.1.3.4.

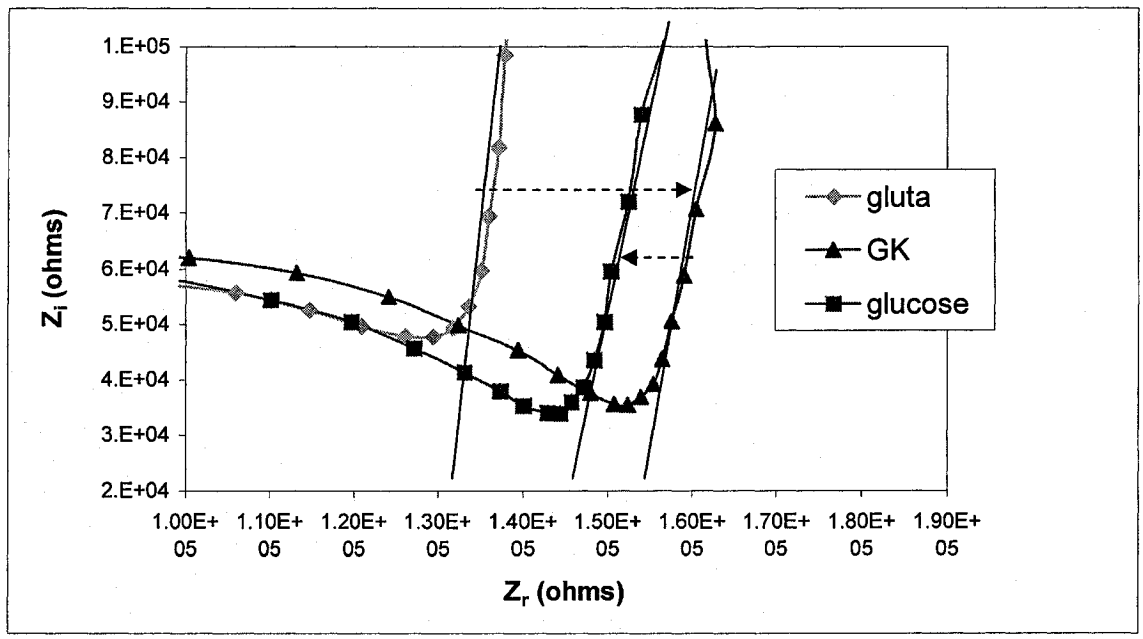

Figure 4.1.3.4: Nyquist plots for glutaraldehyde, immobilization of glucokinase and glucose (100 mM). The concentration of the glucokinase solution was ~ 250 μg/mL.

In figure 4.1.3.4, a strong positive shift of ~ $1.6x10^4$ Ω is observed following the immobilization of the glucokinase. When glucose is then added to the electrolyte, a negative shift of $-7.5x10^3$Ω is observed. These results suggest that the enzyme is immobilized and that the glucose binds to it. However based on the results obtained with

silicon modified with a glucose non-specific enzyme, where a shift is also observed, these results are non-conclusive.

4.1.4. Enzyme activity tests.

Experiments to assess the activity of the immobilized enzyme were performed according to a previously described protocol (performed at the Lady Davis Institute, refer to chapter 3). Table 4.1.4.1 summarizes the resulting data.

	Absorbance at λ = 340 nm (a.u)		
Electrode	**19 min**	**41 min**	**57 min**
Si	0.000	0.002	0.005
SPE	0.000	0.002	0.005

Table 4.1.4.1: Enzyme activity results.

The enzyme activities of one glucokinase modified Si chip and one glucokinase modified SPE electrode were measured. In both cases, enzyme activity is observed through increasing absorbance of NADPH with time. However, the absorbance values are very low. This may be due to two factors:

- This type of test is designed for large amounts of enzyme. The quantity of enzyme immobilized on the electrodes may be too small to be detected with this standard test.
- The enzyme may be rendered inactive once immobilized onto the electrodes.

Loss of enzyme activity would tend to support the need that exists to use relatively high concentrations of glucose to obtain impedance shifts. In fact, it should be reiterated that the method used so far does not ensure that the active site of the enzyme is available to bind the glucose. The coupling is based on the reaction between the NH_2 groups of the enzyme and the aldehyde moieties at the electrode surface. The glucokinase surface possesses numerous NH_2 groups, including in its active site, and any of them could react with the surface (20). The enzyme is thus immobilized in a very random manner. Using this method, there is no way to ensure that the enzyme is bound with its active site directed towards the solution in a manner accessible to glucose.

4.2. Enzyme immobilization using NTA ligand: in-situ generation of diazoniums.

To ensure that the active site remains available after immobilizing the enzyme, a well-known protein purification method: ion metal chelating affinity chromatography (refer to section 3.3.2) was used to functionalize the electrodes. As shown in the flowchart of Figure 3.3.2.4, this approach involves immobilizing the enzyme via two coordination bonds occurring between its histidine tail and the nickel cation. Since the six-histidine tag is placed sufficiently far from the active site, its availability should be greatly enhanced

The first step in adapting this approach to our electrodes was the immobilization of the NTA ligand. Figure 4.2.1 shows a typical cyclic voltammogram obtained at an Si electrode, in an attempt to electrochemically generate a diazonium moiety from the amine group of the ligand .

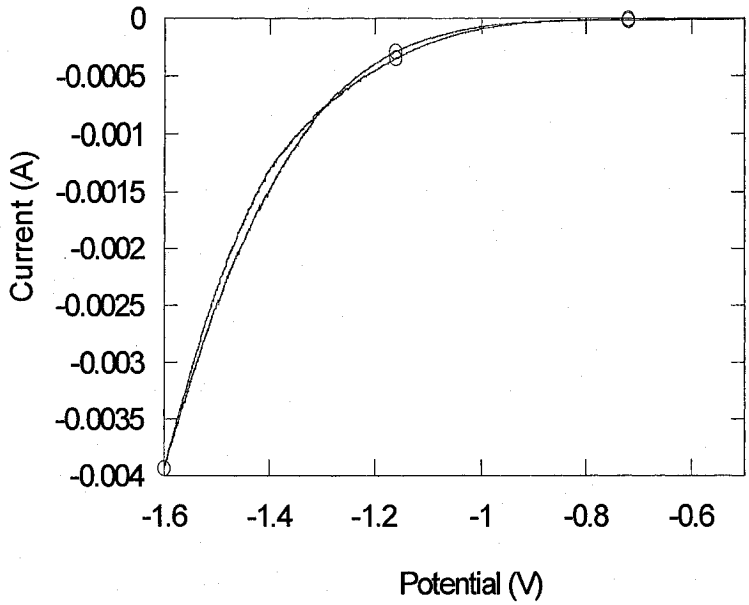

Figure 4.2.1: Cyclic voltammogram obtained for the reduction of the NTA ligand with the Si (111) electrodes. Scan rate: 20 mV/s.

No reduction wave was observed on Si under these conditions, even at scan rates as low as 20 mV/sec. With SPEs however, a small reduction wave could be observed under similar reduction conditions, centered at approximately –1.3 V (Figure 4.2.2). As Figure 4.2.2 illustrates, the voltammograms are somewhat noisy when only 2 of the electrodes of the SPE network are addressed, but substantial improvement occurs when the entire SPE network is used as a single working electrode (significantly increasing the active surface area, Figure 4.2.3). This was done by incorporating the SPE in a traditional three-electrode set-up, with a saturated calomel electrode as a reference and a platinum foil as a counter electrode (refer to figure 3.3.2.5, chapter 3).

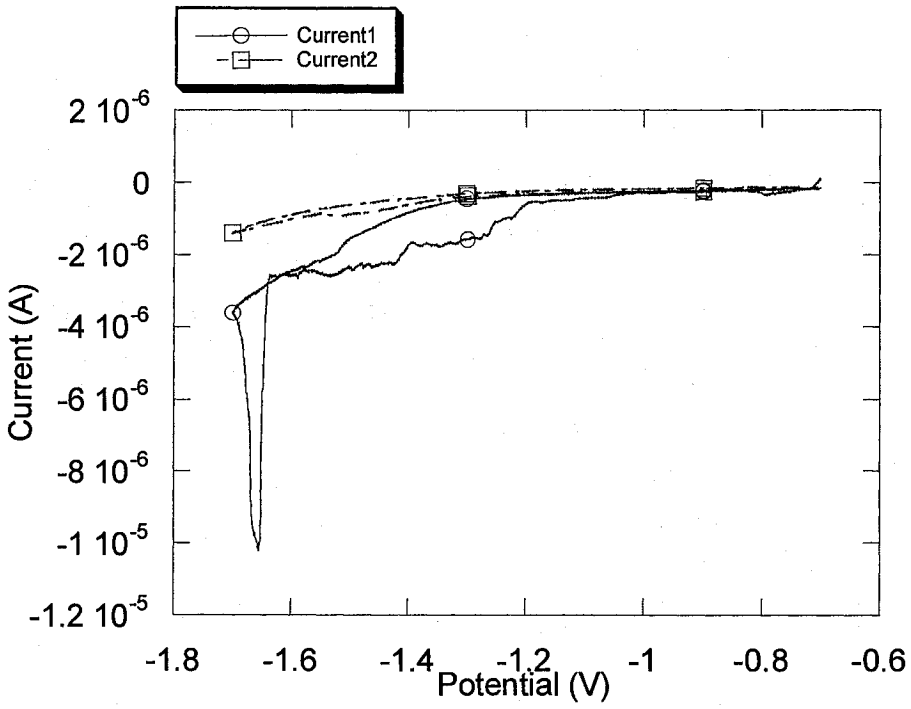

Figure 4.2.2: Cyclic voltammograms obtained for the reduction of the NTA ligand with the SPEs. Scan rate: 20 mV/s.

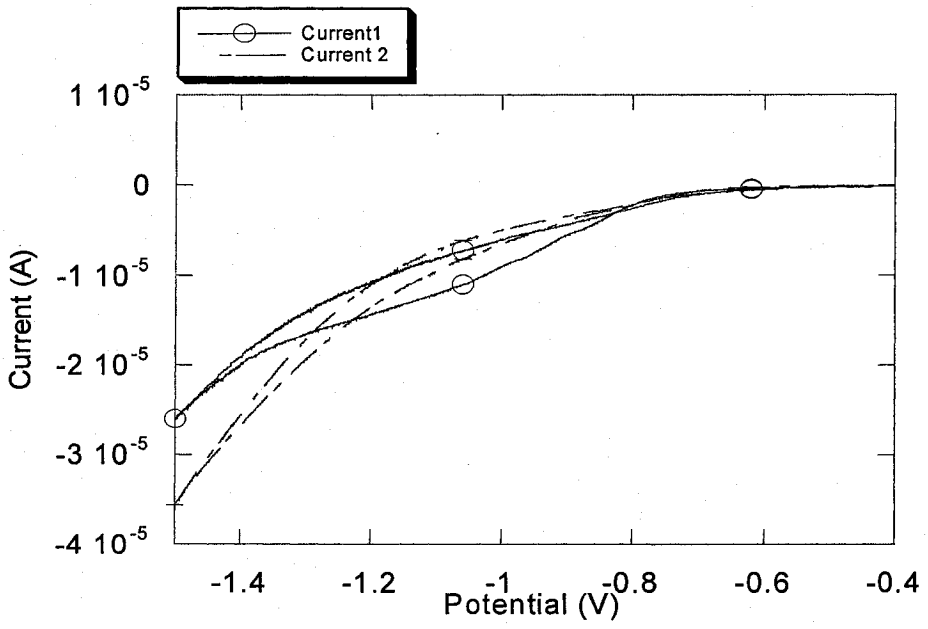

Figure 4.2.3: Voltammograms of the reduction of the NTA ligand when the entire SPE is used as a working electrode.

Following reduction of the ligand onto the SPE surface, these electrodes can be loaded with nickel cations and used to immobilize the enzyme (refer to figure 3.3.2.4). In order to monitor the changes at the surface of the electrode, impedance measurements were taken. Figure 4.2.4 shows the resulting Nyquist plots.

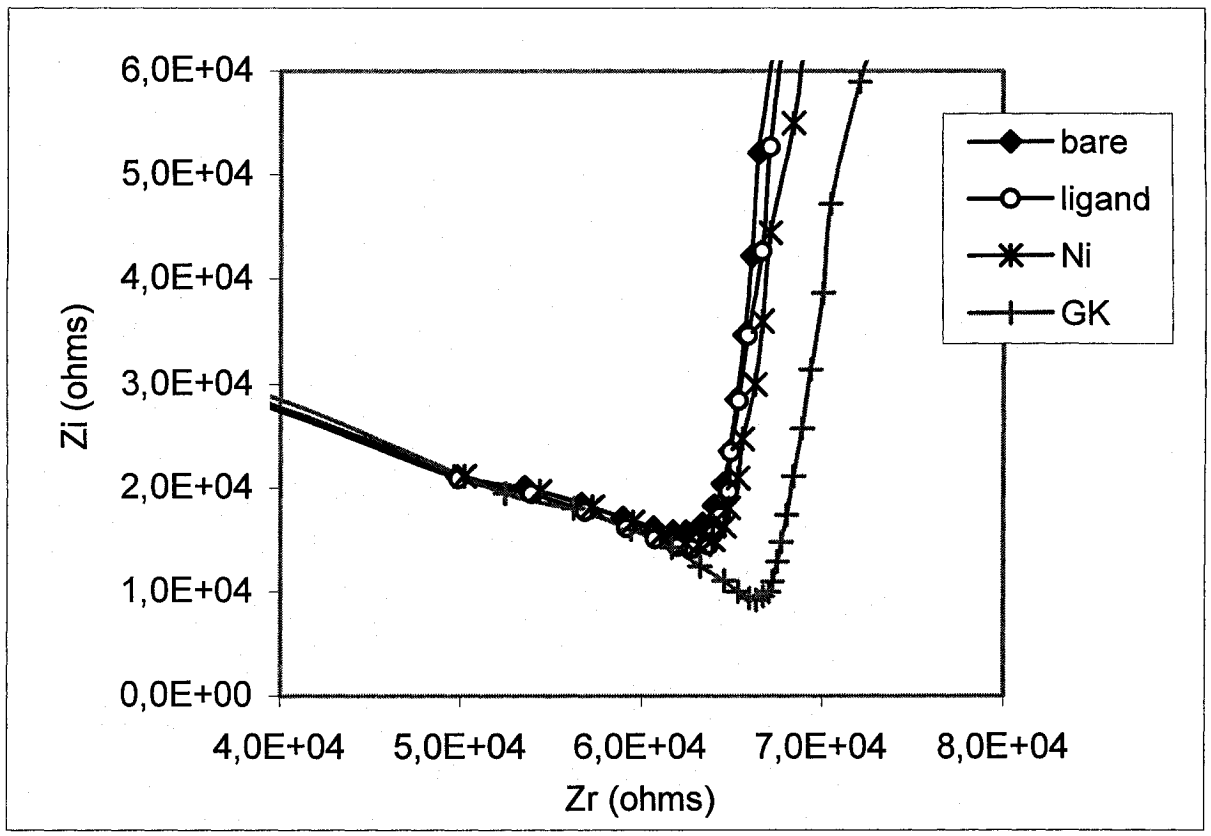

Figure 4.2.4: Nyquist plots for the modification of an SPE with NTA ligand, nickel cation, and glucokinase. (~ 250 µg/mL).

In figure 4.2.4, there is no significant shift between the curves for the bare electrode, after its modification with the NTA ligand, and after charging it with nickel. These results

suggest that the modifications have little effect on the surface of the SPE. The only significant shift was caused by the deposition of the glucokinase (+ $2.3x10^3$ Ω). These plots drive us to the conclusion that there is a very small quantity of ligand that was successfully attached. The shift caused by glucokinase was probably mostly due to its unspecific adsorption onto the electrode.

To verify these conclusions, a solution of a glucose non-specific, non-histidine tagged protein was deposited onto the surface of the SPE, instead of the glucokinase.

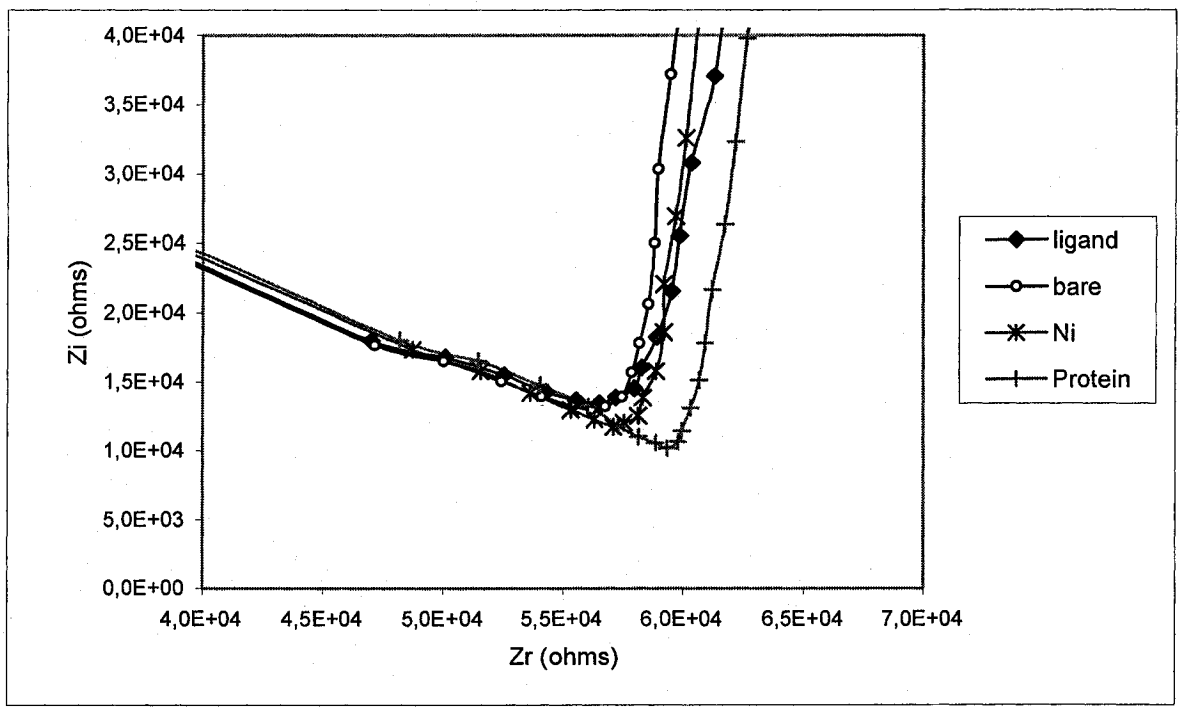

Figure 4.2.5: Nyquist plots for the modification of an SPE electrode with the NTA ligand, nickel cation, and a glucose non-specific protein solution.

As expected, in figure 4.2.5, this non-specific protein caused an impedance shift of $+1.9x10^3\Omega$, which is similar to the shift caused by the immobilization of the 6-histidine tagged glucokinase.

When the glucokinase-modified electrode was put in contact with a solution of glucose, a negative impedance shift of $-1.8x10^3\ \Omega$ was observed which would tend to indicate that the detection approach is working (Figure 4.2.6), but again, is probably mostly due to its unspecific adsorption onto the surface.

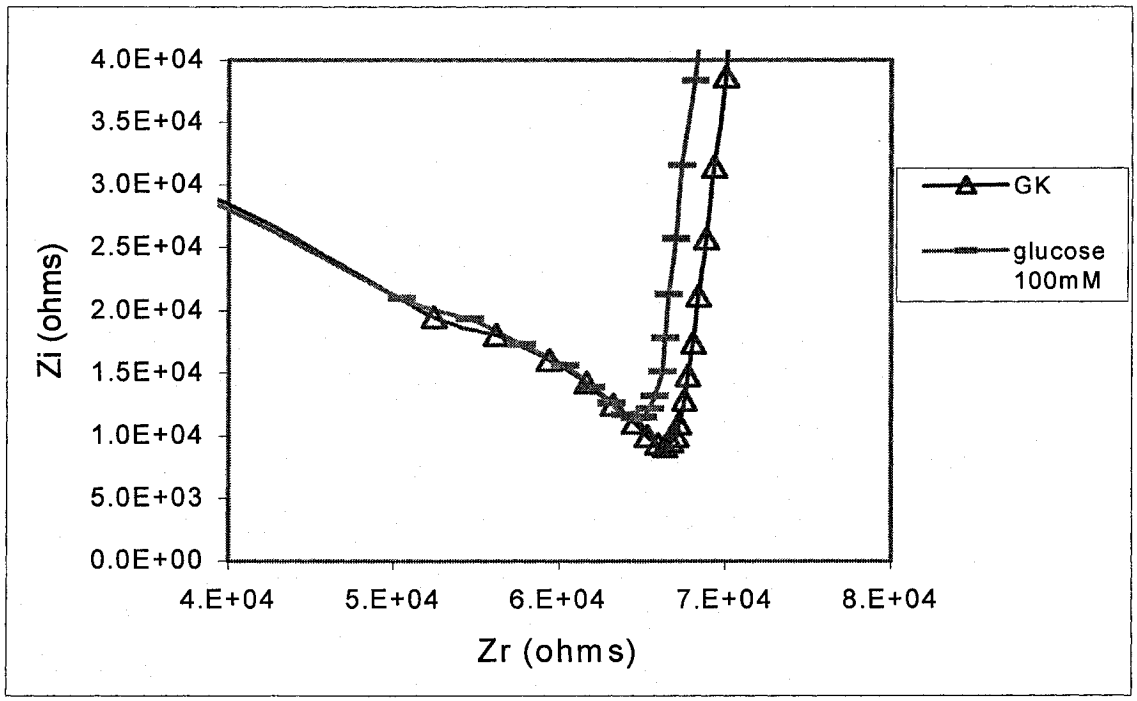

Figure 4.2.6: Nyquist plots for the GK (~ 250 µg/mL). modified SPE in contact with a solution of glucose (100mM).

Enzyme activity tests on the immobilized enzyme were conducted on two modified SPEs and two modified Si (111) chips (Table 4.2.1). The results were compared to a solution of free (non-immobilized) six-histidine tagged glucokinase.

Sample	**10 minutes (a.u)**	**40 minutes (a.u)**	**80 minutes (a.u)**
Free 6-histidine tagged GK	0.074	0.289	0.651
Si (111)	0.000	0.000	0.000
Si (111)	0.003	0.001	0.001
SPE	0.001	0.002	0.001
SPE	0.001	0.001	0.002

Table 4.2.1: Enzyme activity results for the immobilized GK, via the NTA ligand.

In table 4.2.1, the activity of the free 6-histidine tagged glucokinase is observed through the significant increase of NADPH absorbance with time. On the other hand, the immobilized enzyme (whether on Si or SPE) has little activity. Once again, this may be due to two reasons: either the enzyme is inactive after its immobilization, or the amount of immobilized enzyme is below the detection limit of this test. These results are in fact consistent with the voltammograms and the impedance measurements obtained in this section. Indeed, all the data seem to point to the fact that there is very little NTA ligand that was grafted onto the substrates. Consequently, very little enzyme was immobilized.

The inefficiency of grafting the NTA ligand through direct in-situ electrochemical generation of the diazonium moiety may be explained by the following. Successful in-situ generation of diazoniums and their grafting onto solid surfaces has been described in the literature for similar types of molecules (48-52). The difference in the approach presented in this work lies in the structure of the NTA ligand. Electrode modification through the reduction of a diazonium is usually done using a ligand that has the diazonium moiety directly attached to a phenyl ring, just as in the case of the nitrobenzene diazonium used in section 4.1 (53-55). The mechanism of this reduction involves highly reactive radicals (Figure 4.2.2).

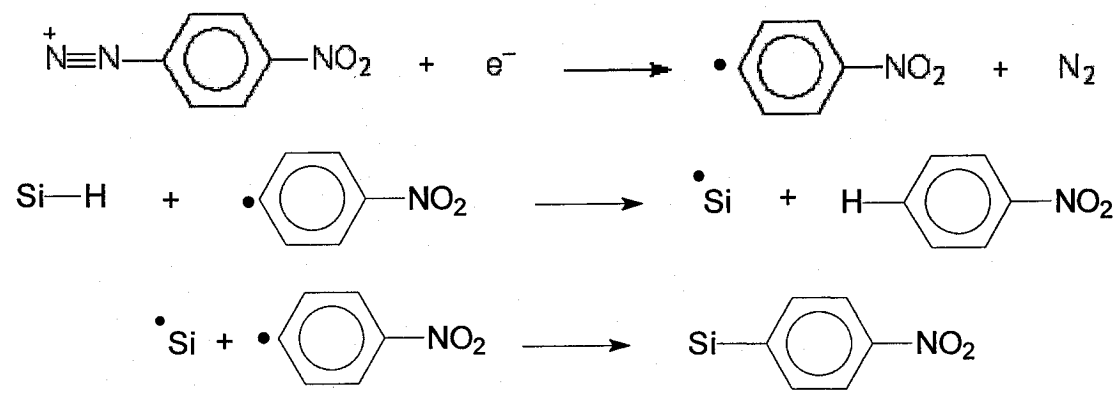

Figure 4.2.2: Mechanism of the grafting of nitrobenzene diazonium onto an Si electrode (9).

The mechanism in figure 4.2.2 shows that the free electron of the generated radical is on the phenyl ring, which stabilizes it by delocalization. In the NTA ligand used for this work, there is no phenyl ring to stabilize such radicals and one may conclude that the reason why electrochemical grafting of the ligand onto the surfaces was unsuccessful is because very few radicals were generated and thus the diazonium moiety could not be easily reduced.

Before moving onto another ligand, another approach to functionalization was attempted, using the same ligand.

4.3. Functionalization of SPEs with EDC for attachment of the NTA Ligand.

In this section, coupling the NTA ligand onto the surface of the electrode was attempted by performing an initial electrochemical functionalization with EDC (refer to figure 3.3.3.1). This was done using chronoamperometry, a technique that resembles cyclic voltammetry where, instead of sweeping the potential, it is kept constant for a certain period of time (23). Figure 4.3.1 shows a typical chronoamperogram obtained for the oxidation of an SPE in the presence of EDC.

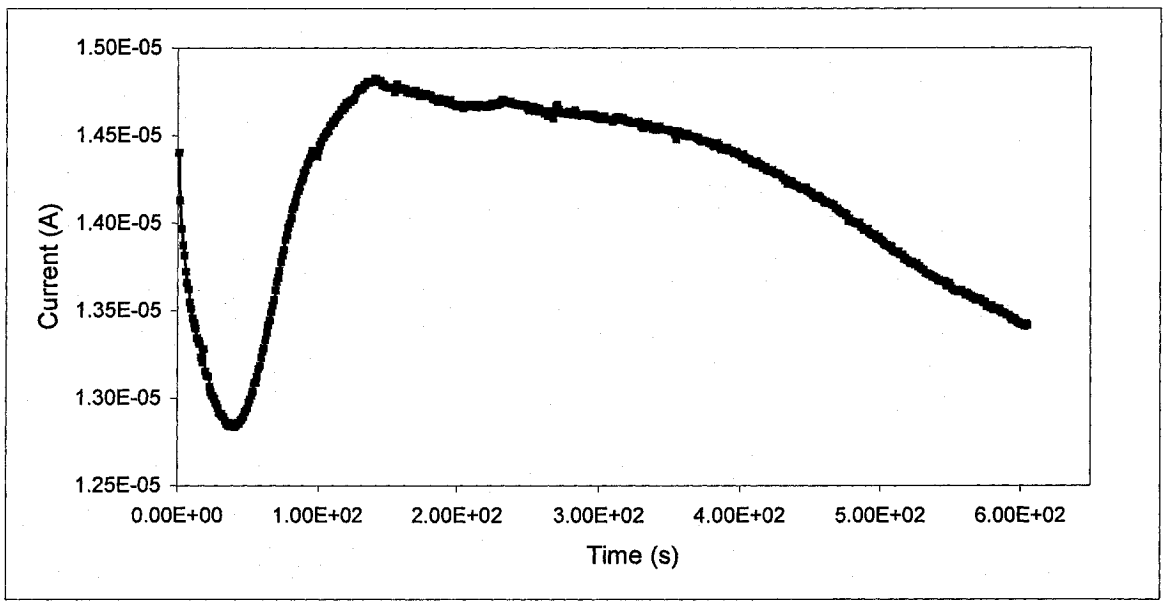

Figure 4.3.1: Chronoamperogram obtained during the oxidation of an SPE in the presence of EDC. Total time: 10 minutes. Applied potential: + 2.2 V.

In figure 4.3.1, an important current wave is observed, showing good reactivity between the electrolyte (containing EDC) and the SPE.

The ligand solution (pH 11) was then deposited for 30 minutes. Impedance measurements were taken after each step (figure 4.3.2).

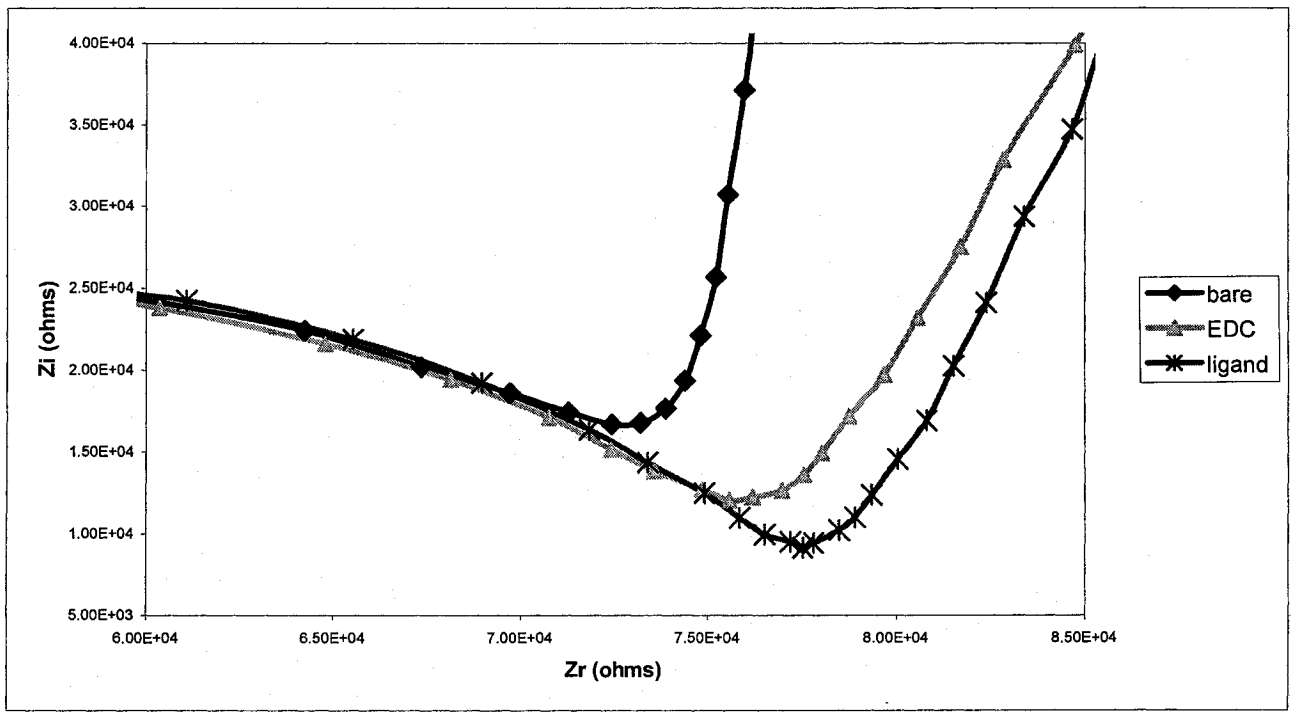

Figure 4.3.2: Nyquist plots of the bare electrode, after its oxidation in the presence of EDC and the addition of the ligand.

In figure 4.3.2, a significant positive shift of 2.0×10^3 Ω between the curve of the bare SPE and the oxidized one in the presence of EDC, is observed. This was to be expected since this step generates an activated ester intermediate (refer to figure 3.3.3.1), which greatly changes the surface of the electrode. After the addition of the ligand, another significant positive shift of 1.1×10^3 Ω is observed. This suggests that the ligand was successfully attached to the electrode.

Control experiments were also conducted to test if direct grafting of the ligand via chronoamperometry, without EDC, would occur. Indeed, since the positive potential and the acidic medium generate carboxylate groups onto the surface of the SPE, it might be possible for the amine moiety of the ligand to form an amide bond with the SPE, without the need for EDC. Figure 4.3.3 shows the resulting chronoamperogram.

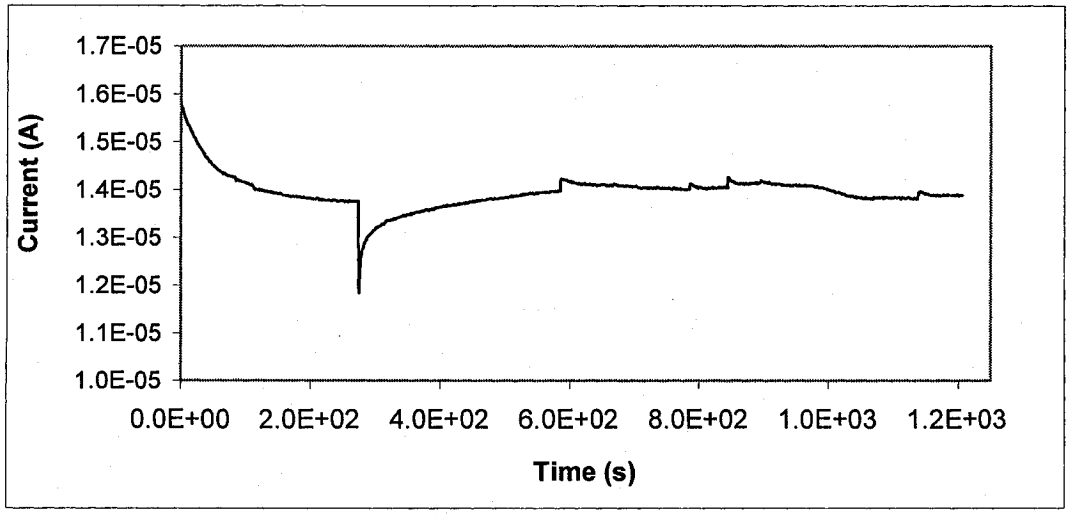

Figure 4.3.3: Chronoamperogram obtained after a chronoamperometry experiment, without EDC. Applied potential: + 2.2V, for 10 minutes.

The chronoamperogram in figure 4.3.3 is very different from the one in figure 4.3.1 as it shows no current wave. The ligand was then deposited and impedance measurements were taken (figure 4.3.4).

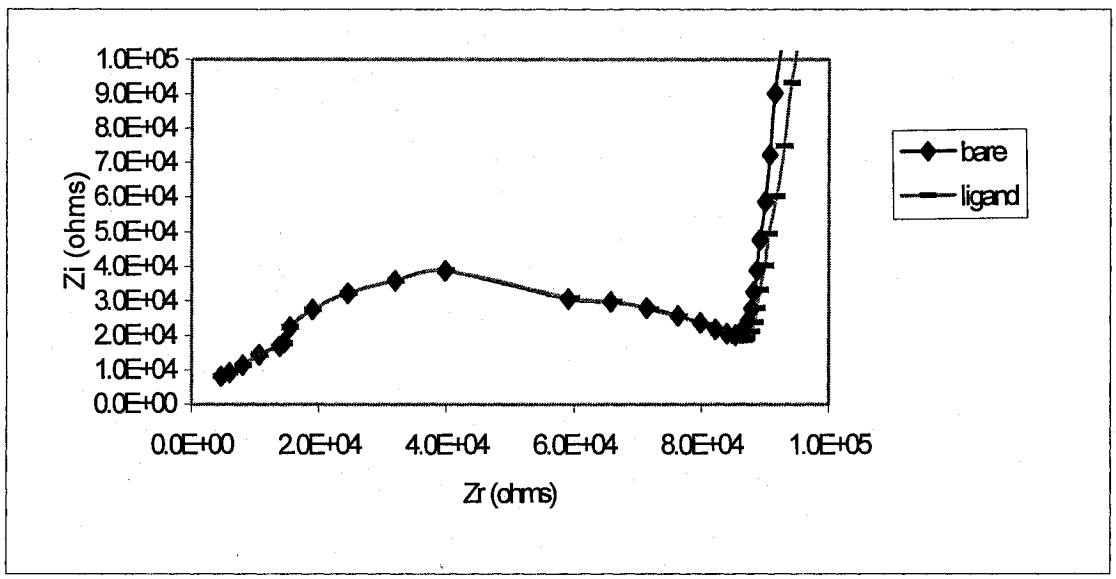

Figure 4.3.4: Nyquist plots for the bare SPE and after its oxidation (in absence of EDC) and deposition of the NTA ligand

In figure 4.3.4, there is a negligible shift before and after the ligand grafting attempt. These results indicate that the latter was unsuccessful. The EDC is thus indispensable for the formation of the amide bond between the oxidized SPE and the amine moiety of the NTA ligand.

Control experiments consisting of depositing the ligand solvent only (solution of $CaCO_3$ at pH 11) onto the electrode, after its oxidation in the presence of EDC, were conducted. An impedance measurement was taken, the ligand solution was deposited (for 30 minutes), and then another impedance measurement was taken. Figure 4.3.5 shows the resulting graphs.

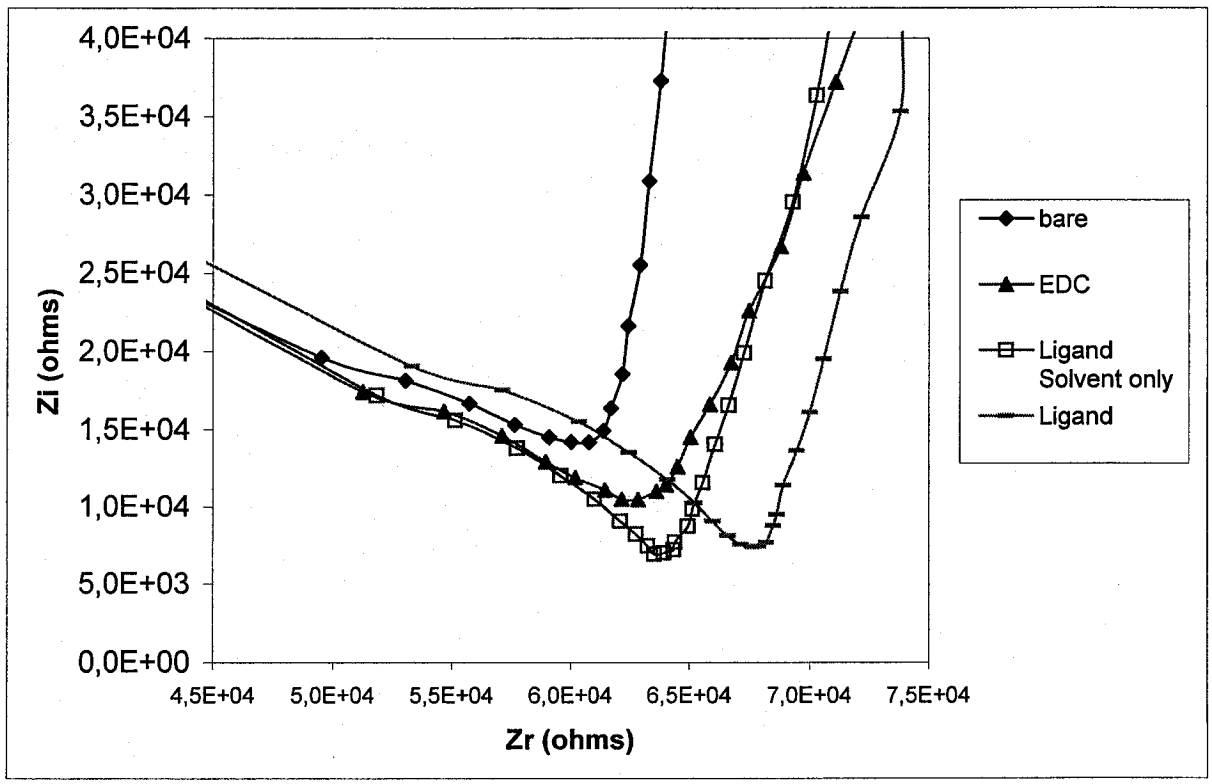

Figure 4.3.5: Control experiment for the modification of an SPE with the NTA ligand.

In figure 4.3.5, a significant positive shift of + $6.1x10^2$ Ω is observed between the curve of the bare SPE and the EDC modified curve. After the deposition of the $CaCO_3$ solution, without the NTA ligand, there is no significant impedance shift, as expected. When the NTA ligand dissolved in $CaCO_3$ was deposited, a significant positive shift of $5.4x10^3$ Ω was observed. These results indicate that the SPE was successfully modified with the NTA ligand.

The next step was the loading of SPE with nickel cation.

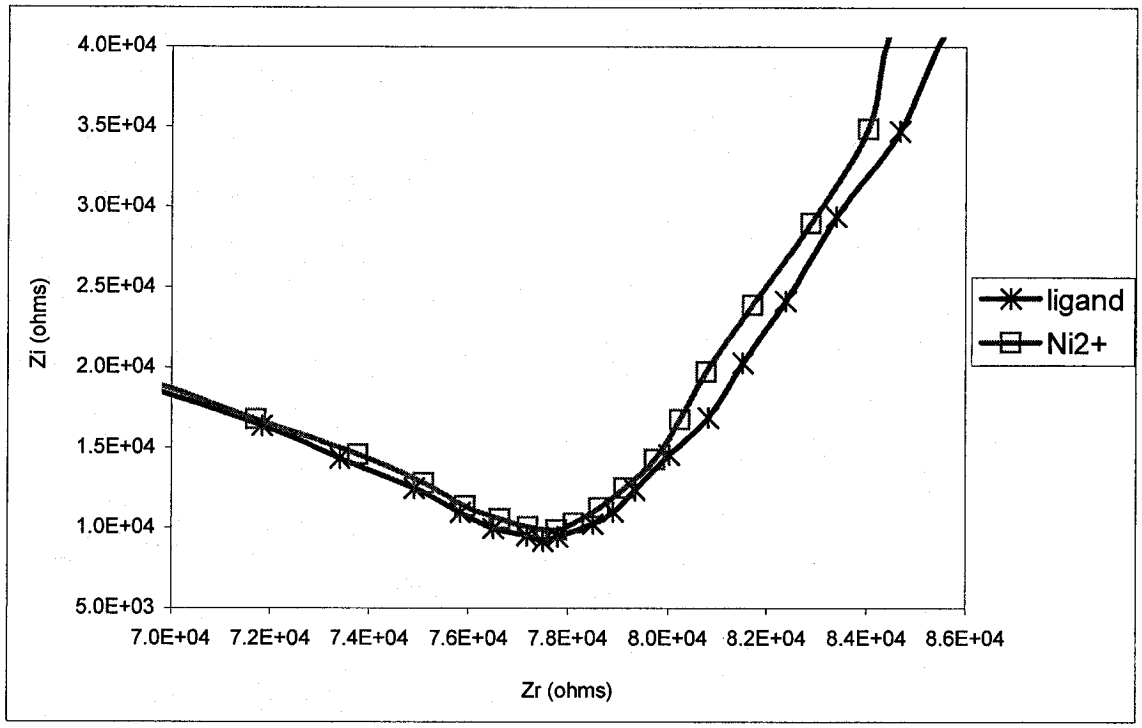

Figure 4.3.6: Nyquist curves for the NTA ligand modified SPE and after it was loaded with Ni^{2+}.

In figure 4.3.6, a small negative impedance shift of –277 Ω, was observed following charging with the nickel. The next modification step was the deposition of the glucokinase (figure 4.3.7).

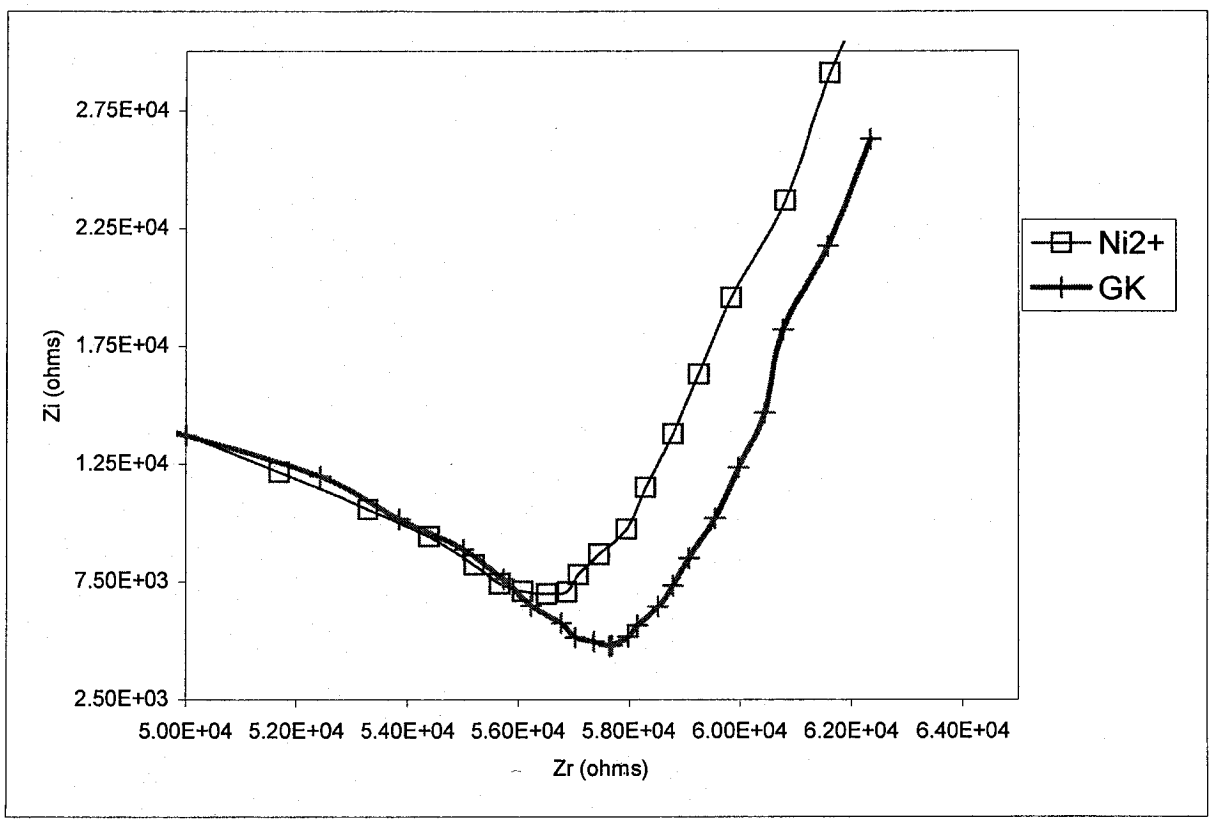

Figure 4.3.7: Nyquist curves for the Ni^{2+} charged SPE and deposition of the glucokinase (~ 250 μg/mL)

In figure 4.3.7, a significant positive impedance shift of $2.2x10^3$ Ω, was observed between the Nyquist plot of the nickel modified SPE and the GK loaded SPE. This shift suggests that the protein was successfully immobilized onto the electrode. To confirm this, another control experiment was run, where only the GK buffer was deposited onto the SPE, for 1 hour. Figure 4.3.8 shows the resulting Nyquist plots.

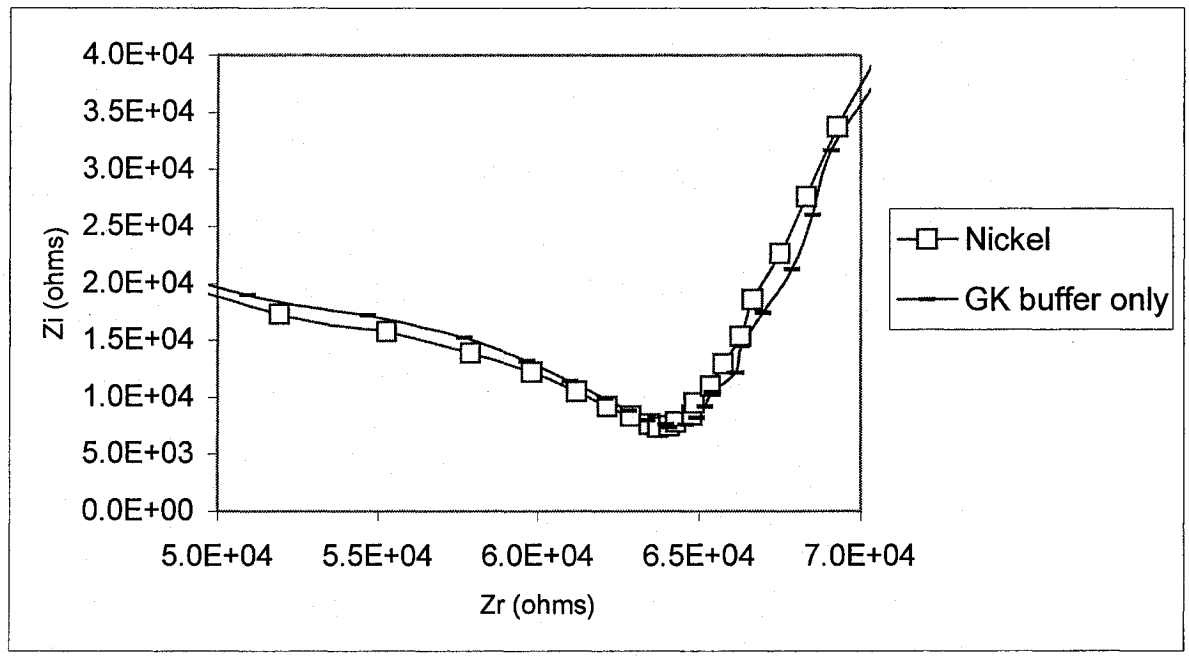

Figure 4.3.8: Nyquist curves for the Ni^{2+} charged SPE and deposition of the glucokinase buffer, only.

In figure 4.3.8, no shift was observed between the curve of the nickel charged SPE and and the curve following deposition of the glucokinase buffer only (without the protein). This data thus tends to confirm that the EDC-based procedure enables the coupling of the glucokinase to the electrode, with the large impedance shifts indicating that an important amount of glucokinase was immobilized.

The final step in the development of this biosensor was putting it in contact with a glucose solution (figure 4.3.9).

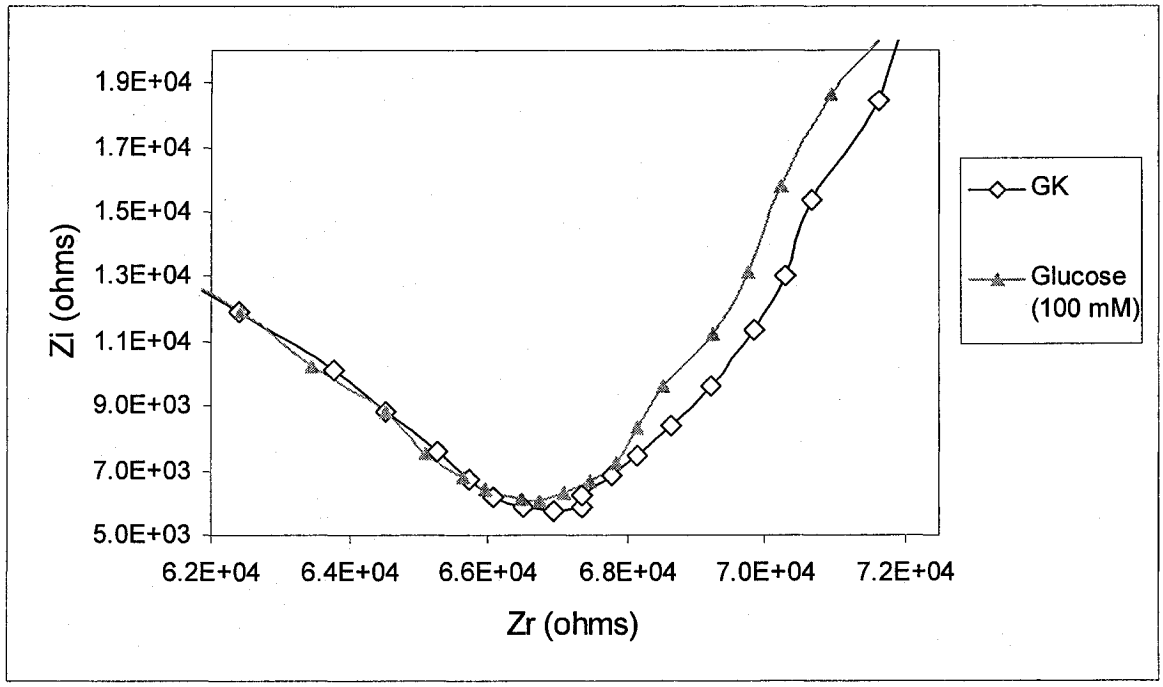

Figure 4.3.9: Nyquist plots of the GK (~ 250 μg/mL) modified SPE and after it was put in contact with a glucose solution (100 mM).

In figure 4.3.9, a negative shift of –223 Ω was observed between the curve of the glucokinase modified SPE and the one where the SPE is put in contact with a glucose solution. Although the shift is small, these results suggest that the glucose is binding to the glucokinase and that the biosensor is able to detect it adequately. However, other experiments should be conducted to confirm that the glucose is binding specifically to the enzyme. For example, a non-specific sugar can be used instead of the glucose (e.g: mannose or fructose). Also, a non-glucose specific protein tagged with a six-histidine tail can be immobilized onto the SPE and put in contact with a solution of glucose.

Chapter 5

Conclusions and Future Work

5.1. Conclusions

The goal of this project was to develop a glucose biosensor using the enzyme glucokinase as the probe molecule, and silicon as well as screen-printed carbon electrodes as the transducer.

The most crucial step was the grafting of the enzyme onto the substrates, without losing its activity. Three methods were thus explored. In the first one, the electrodes were modified using nitrobenzendiazonium, which was then reacted with glutaraldehyde. The latter served as a cross-linker between the electrode and the enzyme. Impedance measurements showed that the latter was immobilized in a random manner, and so the availability of the active site was not always ensured.

In the second immobilization procedure, an amine terminated NTA ligand was used. After its loading with nickel cations, it was expected to bind to the 6-histidine tail that was added to the glucokinase. Generating in-situ diazoniums from the amine moiety in order to electrochemically reduce the ligand onto the electrode proved to be unsuccessful. This was attributed to the lack of a phenyl ring in the structure of the ligand.

In the last immobilization method, the same NTA ligand was grafted onto the electrodes, after their oxidation in the presence of EDC. It was then loaded with nickel cations and the 6-histidine tagged glucokinase was deposited. Impedance measurements indicate that the enzyme was successfully immobilized and that it binds the glucose. However, more control experiments should be conducted to confirm this result.

One important advantage of the device is its short response time: about 7 minutes for a Mott-Schottky plot and 1.5 minutes for a Nyquist plot. The simple procedure that we have developed is promising and presents potential for a reagentless glucose sensor, however, much work needs to be done.

5.2. Future work

The last immobilization method was found to be the most adequate one and so it should be tested onto the Si substrates as well. Furthermore, each step of the preparation of the biosensor, after the oxidation in presence of EDC, needs to be optimized separately:

- Concentration of the NTA ligand and pH of its solvent.
- Concentration of the enzyme. Indeed, a balance between optimum coverage of the surface and steric hindrance between the immobilized enzyme molecules has to be achieved.
- Variation of the concentration of glucose to obtain a calibration curve.

Once the optimization is complete, tests with mutated glucokinase should be conducted.

One important goal is to increase the sensitivity of the sensor. Indeed, we have used a glucose concentration of 100 mM, whereas a more reasonable concentration interval would be 5 - 10 mM, since the sensor is intended for diabetics. There are several ways to achieve this:

- Increase the surface area of the electrode, so that more glucokinase can be immobilized.

- Dr. Trifiro and his research group at the Lady Davis Institute have been working on a new mutated hexokinase that is expected to have much more glucose affinity than the glucokinase. This should have a great impact on the detection limit.

One major problem that stems from the last immobilization procedure is the high cost of the NTA ligand: 440$ / 10 mg. Indeed, there are few commercially available NTA ligands. According to literature, research laboratories usually synthesize their own. During this project, the synthesis of another NTA ligand, 4-aminophenyl-NTA ligand, was initiated in collaboration with Mr. G. Hersant from Dr. Marsan's laboratory at Université du Québec à Montréal. Due to time constraints, it was not possible to complete it. Figure 5.2.1 shows the scheme of the synthesis that was started. The first two steps worked properly, although the obtained yields were lower than expected. The hydrogenation proved to be more difficult to achieve.

This ligand will have several advantages over the one that was used throughout this project (44):

- It has an aniline moiety and so in-situ diazotisation should be easily achievable.
- After the diazotisation, the ligand can be simply reduced onto both types of substrates using cyclic voltammetry.
- Synthesizing it is significantly cheaper than purchasing the Qiagen NTA ligand. Indeed, purchasing all the ingredients only cost about 300 $.

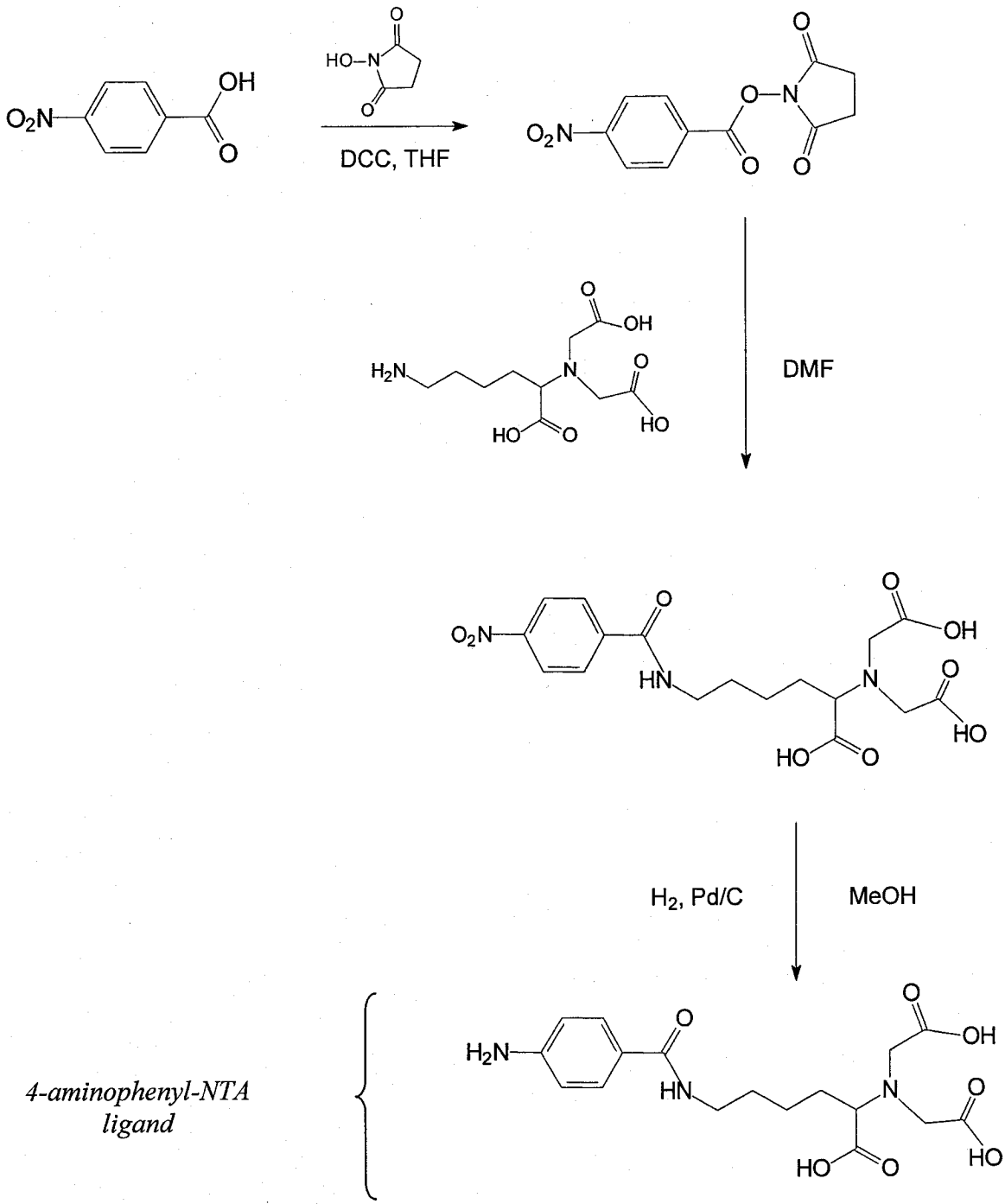

Figure 5.2.1: Synthesis of the 4-aminophenyl-NTA ligand. DCC stands for: 1,3-dicycloheyxlcarbodiimide. (44)

References:

1. K. Bellenier, *Diabetes sourcebook: basic consumer health information about Type 1 diabetes (insulin-dependent or juvenile-onset diabetes), Type 2 diabetes (noninsulin-dependent or adult-onset diabetes), gestational diabetes, and related disorders,* Detroit, MI : Omnigraphics (1999)
2. World Health Organization: http://www.who.int/en/
3. Statistics Canada: http://www.statcan.ca/
4. J.C Pickup, M.A Crook, P. Tutt (1993), *Diabetic Medicine*, 10, 402-411
5. E. Wilkins, P.Atanasov (1995), *Med. Eng. Phys.*,18, 4, 273-288
6. P.U Abel, T. von Woedtke, (2002) *Biosensors and Bioelectronics*, 17, 1059-1070
7. The Diabetes Control and Complications Trial Research Group (1993) *N Engl J Med,* 329, 977-986
8. N. Deligiannis, *DNA Detection System of Homo-oligomers By Electrochemical Impedance Measurements And Quantification Through Radiolabelling,* Concordia University (2000).
9. A. Mak, *Detection Of Oligonucleotides Sequesnces On Diazonium Modified Silicon Substrates Through Electrical Impedance Measurements,* Concordia University (2002)
10. A. Macanovic, *Impedance-Based Detection Of DNA Sequences Using A Silicon Transducer With PNA As The Probe Layer,* Concordia University (2004)
11. P.Vadgama *et al* (1992), Analyst, 117, 1657-1670.
12. Private communications with Dr. M. Trifiro and his research group.

13. Albisser A.M (1979), *The Journal of laboratory and Clinical Medicine,* 7, 515-51

14. SMSIinc (Sensors for Medicine and Science, inc): http://www.s4ms.com

15. T.Mckee, J.R Mckee, *Biochemistry, an introduction,* (1999), WCB/McGraw-Hill.

16. P. M. Woster, *Enzymes-Kinetics and Catalysis (Pharmacetuical Biochemistry I)* http://wiz2.pharm.wayne.edu/biochem/enz.html , Wayne State Universtiy.

17. S. P. Miller *et al* (1999), *Diabetes*, 48, 1645-1661.

18. L. Z. Xhu *et al* (1996), *The Journal of Biological Chemistry*, 270, 17, 9939-9946.

19. B. Mahalingam *et al* (1999), *Diabetes*, 48, 1698-1705

20. K. Kamata *et al* (2004), *Structure*, 12, 426 - 438

21. E. Souteyarand *et al* (1997), *The Journal of Physical Chemistry*, 101, 15, 2980-2985.

22. A.C. Fisher, *Electrode Dynamics*, Oxford Chemistry Primers (1996).

23. A.J. Bard, L.R. Faulkner, *Electrochemical Methods: Fundamentals and Applications*, Wiley New York (2001)

24. M. Grätzel (2001), *Nature*, 414, 338-344.

25. Collaboration through meetings with Dr.M. Lawrence.

26. Gamry Instruments, *Electrochemical Impedance Spectroscopy Primer*, www.gamry.com

27. J.R. Macdonald (1987), *Impedance Spectroscopy: Emphasizing Solid Materials and Systems,* John Wiley & Sons Inc, New York.

28. C.A. Marquette *et al* (2006) *Analytical Chemistry*, 78 (3), 959-964.

29. A.M. Bond (2002), *Broadening Electrochemical Horizons: Principles and Illustrations of Volatmmetric and Related Techniques*, Oxford, New York.

30. I. Wilner *et al*, (2000), *Angewandte Chemie, Internation Edition*, 39 (7), 1181-1218.

31. S. Ferretti *et al*, (2000) *Trends in Analytical Chemistry*, 19 (9), 530 – 540.

32. P. Villeneuve *et al* (2000), *Journal of Molecular Catalysis B: Enzymatic*, 9, 113-148.

33. N. Dale *et al* (2005), *Trends in Biotechnology*, 23, 8, 420 – 428.

34. C.H. de Villeneuve *et al* (1997) *Journal of Physical chemistry B*, 101 (14), 2415-2420.

35. P. Allongue *et al* (1997), *Journal of American Chemical Society*, 119, 201-207.

36. A. Jungbauer *et al* (2004), *Current Opionion in biotechnology*, 15 (5), 487- 494.

37. A. Hidalgo *et al* (2004), *Biotechnology Progress*, 20 (5), 1578-1582

38. J. Porath et al (1975), Nature, 258, 598-599.

39. V. Gaberc-Porekar *et al* (2001), *Journal of biochemical and biophysical methods*, 49 (1-3), 335-360.

40. M.F.G.S. Gillet *et al* (2004), *Protein Expression an Purification*, 33 (2), 256-264.

41. A.K. Mohanty et al (2004), *Protein Expression an Purification*, 33 (2), 311-325.

42. D.F. Westra et al (2001), Journal of Chromatography B: Biomedical Sciences and Applications, 760 91), 129-136.

43. Qiagen Inc website: http://www1.qiagen.com/

44. R. Blankespoor *et al* (2005), *Langmuir*, 21, 3362-3375.

45. G.T. Hermanson *et al*, *Immobillized Affinity Ligand Techniques*, Academic Press (1992).

46. D. Voet et al (2006), *Fundamentals of biochemistry: life at the molecular level, Hoboken, N.J.* , Wiley

47. B. Steve *et al* (2005) *Journal of Physical Chemistry B*, 109 (51), 24401-24410.

48. L. Zuojiang *et al* (2005), *Langmuir*, 21 (25), 11999-12006

49. B. Jeffrey *et al* (2001), *Chemistry of Materials*, 13 (11), 3823-3824.

50. L.M. Martin (1996), *Tetrahedron Letters*, 37 (44), 7921-7924.

51. D. Sheng *et al* (2005), *Chemistry of Materials*, 17 (7), 1717-1721.

52. A.J. Downard (2000), *Electroanalysis*, 12 (14), 1085-1096.

53. M. D'Amours *et al* (2003), *Journal of Physical Chemistry B,* 107 (20), 4811-4817.

54. A. Chaussé *et al* (2002), *Chemical Materials,* 14, 392-400.

55. A. Adenier *et al* (2001), *Journal of the American Chemical Society,* 123, 4541-4549.